# AT-752 targets multiple sites and activities on the Dengue virus replication enzyme NS5

Mikael Feracci, Cécilia Eydoux, Véronique Fattorini, Lea Lo Bello, Pierre Gauffre, Barbara Selisko, Priscila Sutto-Ortiz, Ashleigh Shannon, Hongjie Xia, Pei-Yong Shi, et al.

# Journal Pre-proof

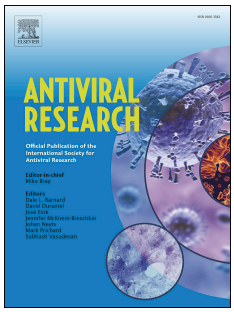


AT-752 targets multiple sites and activities on the Dengue virus replication enzyme NS5

Mikael Feracci, Cécilia Eydoux, Véronique Fattorini, Lea Lo Bello, Pierre Gauffre, Barbara Selisko, Priscila Sutto-Ortiz, Ashleigh Shannon, Hongjie Xia, Pei-Yong Shi, Mathieu Noel, Françoise Debart, Jean-Jacques Vasseur, Steve Good, Kai Lin, Adel Moussa, Jean-Pierre Sommadossi, Aurélie Chazot, Karine Alvarez, Jean-Claude Guillemot, Etienne Decroly, François Ferron, Bruno Canard

PII: S0166-3542(23)00052-9

DOI: https://doi.org/10.1016/j.antiviral.2023.105574

Reference: AVR 105574

To appear in: *Antiviral Research*

Received Date: 20 November 2022

Revised Date: 26 February 2023

Accepted Date: 27 February 2023

Please cite this article as: Feracci, M., Eydoux, Cé., Fattorini, Vé., Lo Bello, L., Gauffre, P., Selisko, B., Sutto-Ortiz, P., Shannon, A., Xia, H., Shi, P.-Y., Noel, M., Debart, Franç., Vasseur, J.-J., Good, S., Lin, K., Moussa, A., Sommadossi, J.-P., Chazot, Auré., Alvarez, K., Guillemot, J.-C., Decroly, E., Ferron, Franç., Canard, B., AT-752 targets multiple sites and activities on the Dengue virus replication enzyme NS5, *Antiviral Research* (2023), doi: https://doi.org/10.1016/j.antiviral.2023.105574.

# AT-752 targets multiple sites and activities on the Dengue virus replication enzyme NS5

Mikael Feracci[1], Cécilia Eydoux[1], Véronique Fattorini[1], Lea Lo Bello[1], Pierre Gauffre[1], Barbara Selisko[1], Priscila Sutto-Ortiz[1], Ashleigh Shannon[1], Hongjie Xia[2], Pei-Yong Shi[2], Mathieu Noel[3], Françoise Debart[3], Jean-Jacques Vasseur[3], Steve Good[4], Kai Lin[4], Adel Moussa[4], Jean-Pierre Sommadossi[4], Aurélie Chazot[1], Karine Alvarez[1], Jean-Claude Guillemot[1], Etienne Decroly[1], François Ferron[1], & Bruno Canard[1]*

[1]AFMB, CNRS, Aix-Marseille University, UMR 7257, Case 925, 163 Avenue de Luminy, 13288 Marseille Cedex 09, France
[2] Department of Biochemistry and Molecular Biology, Sealy Institute for Drug Discovery, Sealy Center for Structural Biology and Molecular Biophysics, University of Texas Medical Branch, Galveston, TX, USA. peshi@utmb.edu.
[3]IBMM, UMR 5247 CNRS-UM1-UM2, Department of Nucleic Acids, Montpellier University, Place E. Bataillon, 34095 Montpellier Cedex 05, France
[4]Atea Pharmaceuticals, Inc.; 225 Franklin St., Suite 2100, Boston, MA 02110 USA.

*Corresponding author: bruno.canard@univ-amu.fr

**Abstract**

AT-752 is a guanosine analogue prodrug active against dengue virus (DENV). In infected cells, it is metabolized into 2'-methyl-2'-fluoro guanosine 5'-triphosphate (AT-9010) which inhibits RNA synthesis in acting as a RNA chain terminator. Here we show that AT-9010 has several modes of action on DENV full-length NS5. AT-9010 does not inhibit the primer pppApG synthesis step significantly. However, AT-9010 targets two NS5-associated enzyme activities, the RNA 2'-O-MTase and the RNA-dependent RNA polymerase (RdRp) at its RNA elongation step. Crystal structure and RNA methyltransferase (MTase) activities of the DENV 2 MTase domain in complex with AT-9010 at 1.97 Å resolution shows the latter bound to the GTP/RNA-cap binding site, accounting for the observed inhibition of 2'-O but not N7-methylation activity. AT-9010 is discriminated ~10 to 14-fold against GTP at the NS5 active site of all four DENV1-4 NS5 RdRps, arguing for significant inhibition through viral RNA synthesis termination. In Huh-7 cells, DENV1-4 are equally sensitive to AT-281, the free base of AT-752 ($EC_{50} \approx 0.50$ μM), suggesting broad spectrum antiviral properties of AT-752 against flaviviruses.

## Introduction

The *Flavivirus* genus includes a number of significant human pathogens, such as Yellow Fever (YFV), Zika (ZIKV), West-Nile (WNV), Tick-Borne Encephalitis (TBEV), Japanese Encephalitis (JEV), and Dengue (DENV) viruses (Pierson and Diamond, 2020). They productively infect the salivary glands of their arthropod vectors, which transmit the virus to humans through subsequent bites during blood-meals. Flaviviruses are enveloped viruses infecting a wide variety of cells through binding to diverse receptors at the host cell surface. Dengue disease outbreaks and associated conditions have devastating public health and economic consequences in afflicted countries. With ~20,000 deaths and more than 100 million cases annually, Dengue morbidity and burden are considerable. DENV designs a group of at least four antigenically distinct members classified as Dengue serotype 1-4, homologous about 70% to each other at the amino acid level in their most conserved NS5 gene (van den Elsen et al., 2021).

The emergence of Zika virus in 2016 and its spreading from the pacific zone to South America and later worldwide illustrates the pandemic potential of either known or yet-to-be discovered flaviviruses (Masmejan et al., 2020). The recent emergence in the USA of Powassan virus (POWV), a BSL-3 deadly tick-borne flavivirus (Doughty et al., 2017), indicates that this viral genus deserves to be surveilled closely as it contains several BSL-4 agents such as, *eg.*, Omsk hemorrhagic fever virus (OHFV), and Kyasanur Forest disease virus (KFDV).

Besides the successful YFV vaccine, JEV and TBE are amongst the few protective vaccines available to contain flavivirus outbreaks. Ideally, DENV vaccine design requires a yet unreached full-protection against all serotypes at once. DengVaxia™, a vaccine approved in several countries, is recommended to persons aged >9 years old, without previous exposure to DENV (www.who.int/publications/i/item/who-wer9335-457-476). More recently, QDENGA™ was approved in Europe and in some endemic countries for individuals 4-years of age and older by preventing 84% of hospitalized Dengue cases but immunity is fading after 4 years, with only 65% protection (Rivera et al., 2022).

The genome size of human pathogenic flaviviruses is in the vicinity of 11 kb. It is made of a single-stranded RNA molecule of positive polarity ((+)RNA), which is 5'-capped but not 3'-poly-adenylated. The absence of a polyA tail is consistent with the functionalities provided by the 5' and 3' end sequences: the latter RNA ends partially anneal and fold into a defined structure promoting cyclization of the genome and a binding platform for the RNA replication/transcription complex (Filomatori et al., 2011). The RTC comprises seven non-structural protein NS1, NS2a & b, NS3, NS4a & b, and NS5. It associates to membranes within vesile-like structures into a viral factory able to produce proviral RNA (van den Elsen et al., 2021). The latter and protein components assemble to form new virions.

NS5 is an RNA-dependent RNA polymerase (RdRp) of ~100 kDa, responsible for viral RNA synthesis, and the most structurally conserved protein across flavivirus members. Along with RdRp activity, it carries both N7-guanine and 2'-O-methyltransferase (MTase) activities involved in the synthesis of a canonical eukaryotic RNA-cap (Ray et al., 2006; van den Elsen et al., 2021). In the eukaryotic cell, RNA capping proceeds through three reactions occurring onto the neo-transcribed RNA (Ramanathan et al., 2016). The nascent 5'-triphosphate transcript is first converted to the 5'-diphosphate by an RNA triphosphatase. The flavivirus NS3 helicase possesses this activity, although this has never been demonstrated as being involved in the RNA capping process. The 5'-diphosphate RNA transcript is then capped by the addition of GMP originating from GTP by a guanylyltransferase (GTase). The flavivirus NS5 is suspected to carry this activity,

yet the active site, catalytic residues, and mechanism of the reaction remain elusive (El Sahili and Lescar, 2017). The capped RNA is then sequentially methylated both at the N7-guanine of the guanine cap and then the 2'-hydroxyl of the first transcribed nucleotide, a flavivirus-conserved adenosine at position 1 (Ray et al., 2006).

Although Dengue outbreaks have been plaguing the tropical/subtropical belt for decades, the COVID19 crisis brought increased awareness and progress in the potential control and management of pandemic viruses. In particular, prophylactic and therapeutic antiviral drugs have been deemed useful together with the requirement of both rapid diagnostics and auxiliary treatment as early as possible after infection.

Fortunately, such diagnostics exist for Dengue, in particular in the early detection of minute amounts of NS1 in the bloodstream of infected individuals. The amount of NS1 correlates with disease severity (reviewed in (Ghetia et al., 2022)): the severity of the disease has been shown to be positively co-related to the height of the post-infection viremia peak. Therefore, as for many other serious infectious diseases caused by an RNA virus, there is a renewed interest in the design of potent antiviral drugs. The recent discovery of potent pan-flavivirus inhibitors targeting NS4b confirms the renewed interest in drug discovery and design against this important virus family (Kaptein et al., 2021; Moquin et al., 2021; Wang et al., 2022), which would likely benefit from combination therapies, as well as with concomitant addressing of the related cytokine storm occurring when virus titers have significantly declined (Kuczera et al., 2018).

NS5 represents a target of choice for antiviral drugs, and in particular nucleoside/tide analogues (NAs). At least four decades of research and many successful clinical developments have contributed to a wealth of knowledge of these drugs. A phylogenetically close relative to DENV, Hepatitis C virus is eradicated from infected individuals with a success rate close to 100% using sofosbuvir-containing combinatorial regimen (Dousson, 2018). Sofosbuvir is an uracil phosphoramidate prodrug converted intracellularly to its 5'-triphosphate form. Its 2'-fluoro, 2'-methyl modified ribose does not impede selection at the HCV NS5b (the RdRp) active site. However, once incorporated and although it contains a 3'-OH, chain termination occurs. It competes with intracellular UTP, and is a non-obligate chain terminator NA promoting accurate chain termination in lieu of UTP.

AT-752, AT-281, and their diastereoisomer bemnifosbuvir (AT-527) are NAs bearing the same 2'-modified ribose and 5'-phosphoramidate motifs as sofosbuvir ~~(Fig. 1A)~~. AT-752 is active against DENV and yellow fever viruses (Good et al., 2021a; Lin et al., 2022), and bemnifosbuvir against both HCV and SARS-CoV2 (Good et al., 2021b, 2020; Shannon et al., 2022). Both drugs are currently under evaluation in clinical trials (https://clinicaltrials.gov/). Neither AT-752 nor bemnifosbuvir carries a natural nucleobase but a *N*-methyl diaminopurine base instead. Upon cell entry, both follow the same metabolism scheme as sofosbuvir up to recover an unsubstituted 5'-monophosphate (Murakami et al., 2014). At that point, though, the ADALP1 enzyme supposedly deaminates the $N^6$-methyl diaminopurine moiety into guanine, and the resulting 2'-fluoro, 2'-methyl ribose guanosine 5'-monophosphate is converted to the 5'-triphosphate (AT-9010). The corresponding 5'-triphosphate of AT-752, ie., AT-9010, is used as a substrate by the DENV2 NS5 (Good et al., 2021a).

In the present paper, we characterize the in vitro antiviral activity of AT-281, the free base form of the hemi-sulfate salt AT-752, against DENV1-4 and investigate the mechanism of action of the active triphosphate metabolite AT-9010 towards various DENV NS5 domains and full-length products of all four serotypes. We show that AT-752 has a broad spectrum antiviral activity in cells infected with DENV1-4. In parallel, AT-9010 shows a dual mode of action on flavivirus

NS5. AT-9010 binds to the RNA-cap binding site of NS5, inhibiting the RNA 2'-O-MTase activity. We report the crystal structure of AT-9010 in complex with the DENV MTase domain at 1.97 Å resolution, accounting for the observed MTase inhibition. Additionally, AT-9010 is barely incorporated during synthesis of the dinucleotide primer pppAG: although acting as a *bona fide* chain terminator, it does not significantly inhibit pppAG formation. However, AT-9010 competes more efficiently with GTP during RNA elongation than sofosbuvir-5'-triphosphate (SOF-TP) with UTP. We show that AT-9010 substrate and inhibitor properties are valid across all DENV1 - 4. Its guanine base is responsible for its bonified substrate properties relative to sofosbuvir, and thus suggests that AT-752 may achieve broad-spectrum clinical benefit in the control of *Flavivirus* infections.

## Results

The nucleoside analogue AT-752 is a purine nucleotide analogue phosphoramidate prodrug which is metabolized intracellularly into AT-9010, a 5'-triphosphate guanosine analogue inhibitor (Good et al., 2020). The natural nucleotide GTP is a substrate used as a building block for many different reactions involving the viral RdRp NS5 along the flaviviral life cycle. Since AT-9010 is a GTP analogue, it could theoretically target both the viral helicase NS3 to fuel motion along RNA and NS5. However, NS3 is able to hydrolyse all NTP unspecifically (Benarroch et al., 2004), and thus, we surmise that it is unlikely that AT-9010 would selectively and efficiently inhibit this process. NS5 likely is the main target of this inhibitor.

GTP is used by NS5 as *i)* the second nucleotide of the strictly conserved pppApG 5'-end of both the (-) and the (+)RNA strands, which can be synthesized even in the absence of a template in the NS5 RdRp active site (Selisko et al., 2012), *ii)* a component of the RNA cap m7GpppApG, *iii)* one of the four nucleotides assembled into the genomic and anti-genomic strand during RNA synthesis of the flavivirus RNA genome.

Figure 1 depicts five putative reactions which could be impeded in the presence of a GTP analogue such as AT-9010, defining possible inhibitory interferences, and thus, a possible mode of action of AT-752/AT-9010 against DENV.

### *AT-752 is a broad-spectrum DENV inhibitor*

We tested the in vitro antiviral activity of AT-281, the free base form of AT-752, using DENV 1–4 that were modified to contain a nano luciferase reporter (see Materials and Methods). Solutions of AT-281 rather than AT-752 were tested to avoid any effect on the pH of the assay that the salt might have had. AT-281 demonstrated potent activity against all four serotypes, with respective $EC_{50}$ values of 0.57, 0.30, 0.75, and 0.57 µM for DENV1, -2, -3 and -4 reporter viruses, respectively, in Huh-7 cells (Fig. 2).

In order to understand the AT-752 molecular basis of action, we set-out to investigate if its active form AT-9010 could compete with GTP in NS5-mediated reactions involved in RNA synthesis of the Dengue RNA genome.

### *AT-9010 binds to both MTase and RdRp domains of Flavivirus NS5*

In order to determine the AT-9010 inhibition effect on all four serotypes DENV1-4, we purified individually three active forms of the DENV NS5 protein, namely the full-length enzyme NS5, and its two functional domains MTase and RdRp. On these three enzymes, we tested their GTP-binding properties in comparison with that of AT-9010 and sinefungin, a known inhibitor of the MTase activity (Lim et al., 2015). Thermal denaturation temperatures were monitored with a thermal shift assay, which records the increase of thermal stability of a given protein/enzyme when bound to its ligand (substrate or inhibitor).

Figure 3 and Table 1 show that for all DENV serotypes, all MTase, RdRp, and NS5 enzymes bind GTP and AT-9010 ($\Delta Tm \geq +2°C$). Sinefungin accordingly does not bind to the RdRp domain (Table 1, panel 2). GTP appears to promote an average 5°C increase in melting temperature to both NS5 and MTase, similar to that of AT-9010. We note that AT-9010 provides to the RdRp domain a greater thermal stability than GTP for all DENV serotypes (≥1°C). Interestingly, there is a functional GTP/AT-9010 RdRp binding site even in the absence of an RNA primer:template.

This finding is consistent with previous work reporting synthesis of the pppApG primer in the presence of $Mn^{2+}$ but absence of an RNA template (Selisko et al., 2012).

In order to determine the mechanism of action of AT-9010 and see on which target its activity predominates, we assayed the different NS5-associated enzymatic activities successively, and evaluated their propensity to be inhibited by AT-9010. We first addressed the MTase domain.

*AT-9010 binds to the NS5 MTase domain and inhibits RNA 2'-O-methylation*

Inhibition was detected in a 2'-O-MTase assay using the MTase domain of DENV2 NS5 and $^{m7}GpppAC_4$ as a substrate. After mixing DENV2 NS5 MTase with increasing concentrations of compound, MTase activity was measured by a filter-binding assay (FBA). We subsequently performed a dose-response assay to evaluate the inhibition profile of AT-9010. We included the compound AT-9002, which carries a hydroxyl group instead of the fluorine atom at its 2'-position (Fig. 1). The $IC_{50}$ of the compounds, deduced from the Hill slope equation (Y=100/(1+((X/$IC_{50}$)^Hillslope) curve-fitting is 4.1 µM $\pm$ 0.4 for AT-9002 and 29.6 µM $\pm$ 2 for AT-9010 (Fig. 4A). Beside confirming the inhibitory activity of the latter, this indicates that the 2'-OH group probably makes a favorable interaction relevant to the inhibition mechanism of the 2'O-MTase activity.

To understand the molecular basis of the inhibition observed in DENV MTase assays, we performed crystallization studies using the isolated, enzymatically active flavivirus MTase domain. Crystals of DENV3 MTase were grown (Barral et al., 2013), soaked into a solution containing 1 mM AT-9010, and the structure was solved using molecular replacement (Table 2).

Figure 4 detail the atomic contacts of AT-9010 bound to the cap-binding pocket of the DENV3 NS5 MTase domain (Fig. 4B). Unlike for GTP in other structures ((Egloff et al., 2002), for a review, see (Lim et al., 2015)), all three phosphate group densities are perfectly defined, including water molecules making specific contacts with their oxygen substituents (Fig. 4C, D). The AT-9010 molecule is a close mimic of GTP, which binds in a position superimposable to that of AT-9010 (Fig. 4E). Interestingly, the 2'-F, 2'-C-methyl groups that distinguish the analogue from its natural GTP counterpart do not alter the ribose pose. The side chain of Lys14, however, is pointing towards the fluorine atom. Lys14 is clearly the 'ribose check' residue, since in other structures (eg., PDB: 5DTO), it makes simultaneous contacts with the 3'- and the 2'-hydroxyls of the GTP cap, at 2.7 and 2.4 Å, respectively. Here, the fluorine atom does not engage into a hydrogen bond, the distance is kept at 3 Å. Similar to GTP, AT-9002 presumably establishes hydrogen bonds with both its 3'- and 2'-OH, explaining the 10-fold lower $IC_{50}$. Likewise, the side chain of Asn18 could provide an unfavorable interaction, but its contact atoms are at a distance of 3.3 Å, thus presumably escaping any significant discrimination from GTP at the binding step.

Interestingly, we did not detect any significant inhibition of the RNA-cap N7-guanine MTase activity at concentrations of AT-9010 up to 1mM using an unmethylated $GpppAC_4$ RNA substrate (not shown). This indicates that the GTP/cap-binding mode used when the N7-guanine is poised to receive the methyl group is different from the one observed here, or in other words, N7-methylation by another MTase domain in *trans* is unlikely.

We conclude that AT-9010, whose concentration builds up to hundreds of micromolar in exposed cells (Good et al., 2020), likely interferes with RNA capping through inhibition of the NS5 MTase domain.

*AT-9010 does not compete significantly against GTP during dinucleotide primer (pppApG) synthesis*

The RdRp domain is able to catalyze both *de novo* primer synthesis and elongation of RNA. We thus investigated how AT-9010 impacts the nucleotide polymerization activities at play at the RdRp active site. To start RNA synthesis from the 3'-end of either (+) genomic or (-) antigenomic strand of the genome, DENV NS5 harbors a *de novo* RNA synthesis activity: the enzyme synthesizes a dinucleotide primer, pppApG, whose sequence is strictly conserved within the *Flavivirus* genus (Selisko et al., 2012). RNA synthesis starts using the very last nucleotide of the genome and antigenome RNA as a template. We have shown before that pppApG is formed in the presence of $Mg^{2+}$ and more efficiently of $Mn^{2+}$ as catalytic ions, the latter even supporting pppApG synthesis in the absence of template. In order to test the effect of AT-9010 on *de novo* initiation we used a short oligonucleotide (AACAGGUUCU) corresponding to the 3'end of the DENV2 genome as a template directing synthesis of pppApG, pppApGpA and pppApGpApA in the presence of ATP and GTP. Figure 5A shows PAGE analysis of reaction products with ATP (with radioactive [$\gamma$-$^{32}$P]-ATP as a tracer), GTP and/or AT-9010 at given concentrations.

As expected in the presence of ATP, GTP and $Mn^{2+}$ we observe the efficient formation of pppApG to pppApGpApA, as well as of pppApA to a minor extent. *De novo* initiation is less efficient in the presence of $Mg^{2+}$ and renders mainly pppApG. When only ATP and AT-9010 are present, with $Mn^{2+}$, more pppApA is formed but also the dinucleotide pppApAT-9010 which is not further extended. AT-9010 thus acts also in the presence of $Mn^{2+}$ as a *bona fide* chain terminator. We quantified the pppApAT-9010 band formation, compared it to pppApG and found that GTP is around 100 times more efficiently incorporated than AT-9010.

In the presence of $Mg^{2+}$, we do not observe any formation of pppApAT-9010. When using increasing concentrations of AT-9010 in the presence of 100 µM GTP we observe inhibition of pppApG formation (Fig. 5A). Quantification of product bands (Fig. 5B) allows the determination of $IC_{50}$ values of ~ 315 µM and ~107 µM in the presence of $Mn^{2+}$ and $Mg^{2+}$, respectively.

We conclude that AT-9010 is strongly discriminated against upon *de novo* initiation by DENV RdRp in comparison to the elongation step (see below). We measured a weak inhibitory effect of AT-9010 on pppApG formation. Our results suggest that the observed anti-*Flavivirus* effect of AT-752 is not significantly based on inhibition of primer pppApG synthesis.

*AT-9010 is a non-obligate chain terminator discriminated 9-to-14-fold towards its natural GTP counterpart by NS5 from all four DENV serotypes*

A ~12-fold discrimination of AT-9010 relative to GTP has been measured previously at the DENV2 NS5 active site during RNA elongation (Good et al., 2021a). We set up experiments to determine the AT-9010 chain terminator activity spectrum against all four DENV serotypes in experiments measuring competitive nucleotide incorporation as well as single nucleotide incorporation.

For the first set-up, the DENV NS5 of individual serotypes 1-4 was bound to a DENV2 specific primer/template combination corresponding to 10 nt of the 5'end of the genome ($P_{10}$) annealed to 20 nt of the 3'end of the antigenome ($T_{20}$) (Good et al., 2021a). This $P_{10}/T_{20}$ combination allows incorporation of GTP at specific positions (here, at position +5, +7, and +8 on the RNA template). The binary complex NS5.$P_{10}/T_{20}$ was challenged with a nucleotide mix containing various ratios of AT-9010 versus GTP. The discrimination against AT-9010 can then be determined by

quantifying at each G /AT-9010 position the percentage of readthrough bands in relation to the percentage of the AT-9010 band multiplied by the concentration ratio of AT-9010 to GTP.

A typical result is shown for DENV4 NS5 in Figure 6A. First, in absence of GTP (three reactions on the left part of the gel) we show that AT-9010 is incorporated and acts as a chain terminator. When increasing AT-9010 concentrations are used in presence of GTP the AT-9010 band at position +5 clearly accumulates (right part of the gel). The quantification of percentage of the readthrough bands versus the AT-9010 band at this position, resulted in a ~14-fold discrimination against AT-9010 versus GTP. The experiments were replicated for all four serotypes (Supplementary Fig. 1A and 1B). Whereas all incorporated AT-9010 in a similar way, determination of discrimination was difficult when the overall activity was less, as for DENV1 and DENV3 NS5. Therefore, we turned to single nucleotide incorporation experiments (see below). Notably, AT-9010 bears chemical resemblance to the activated form of sofosbuvir (2'-F, 2'-C-methyl uracil 5'-triphosphate (SOF-TP)). Sofosbuvir is used as a potent treatment against viral hepatitis caused by the related *Flaviviridae* HCV. SOF, however, shows in infected cells an approximately 20-fold higher $IC_{50}$ activity against DENV compared to HCV (Good et al., 2021a, 2020). We thus repeated this experiment using the same $P_{10}/T_{20}$ system where SOF-TP is potentially incorporated at positions +2 and +6, but as expected did not detect any significant use of SOF-TP (not shown).

In order to determine discrimination of AT-9010 for all four DENV NS5 proteins we used a second set-up of single nucleotide incorporation. We compared the relative incorporation efficiencies of AT-9010 (and AT-9002) relative to GTP at position +1 of a non-specific RNA $P_{10}/T_{20}$ system allowing the incorporation of G as the first nucleotide, using the NAs or GTP as the sole nucleotide at the same concentration. The same design but employing another non-specific RNA $P_{10}/T_{20}$ system allowing the incorporation of U as the first nucleotide was used for SOF-TP and UTP. Figure 6B shows comparative incorporation into RNA of AT-9010 and AT-9002 relative to GTP, as well as SOF-TP relative to UTP using DENV4 NS5 (see Supplementary Figures 2 and 3 for the other serotypes). Steady-state initial incorporation rates were determined (Supplementary Fig.3). The NAs and natural NTP incorporation rates were used to calculate their ratio corresponding to the preference for the natural NTP or the discrimination of NAs relative to their natural nucleotide counterpart (Table 3). None of the NAs are better substrates than their natural nucleotide counterparts. AT-9010 is discriminated against GTP about 11-fold. The efficiency of incorporation of AT-9010 is highest and that of SOF-TP is lowest amongst these three analogues. Being discriminated >100 fold relative to UTP, the pyrimidine base of SOF-TP is probably a key factor driving a loss of potency as a substrate analogue for NS5 compared to AT-9010 (see discussion). Contrary to the MTase inhibition assay, AT-9002 is not performing better than AT-9010 as a RdRp substrate.

Given that AT-752 can be activated to hundreds of micromolar concentrations of AT-9010 in various cells (Good et al., 2020), this indicates that the NA should be incorporated significantly in the ~11 kb DENV genomes during virus replication, and act as a broad spectrum anti-DENV-and anti-*Flavivirus* agent.

*Active-site structural comparison of Hepacivirus, Flavivirus, and Coronavirus RNA polymerases*

AT-9010 is a nucleotide analogue active against three different viral RdRps, those of HCV NS5b (Good et al., 2021b, 2020), DENV1 to 4 NS5 (Good et al., 2021b, and this work), and SARS-CoV-

2 nsp12 (Shannon et al., 2022). There are commonalities in the active site of these viral RdRps (Peersen, 2019), and they translate into an amino-acid sequence conservation around the catalytic center. For all these RdRps, the chemical reaction allows templated ribonucleotide addition at the RNA 3'-end using a common metal-dependent phosphoryl transfer mechanism.

There are, however, subtle amino acid changes in the conserved Motifs A to G of each viral RdRp, which *in fine* translate into the different NA discriminations measured against their natural NTP. In particular, the inefficient substrate properties of SOF-TP towards both SARS-CoV-2 RdRp (Shannon et al., 2022) and DENV1 to 4 NS5 is puzzling (Potisopon et al., 2017, and this work). SOF-TP is an efficient UTP analogue substrate for the HCV RdRp, which bears significant structural homology with DENV NS5.

Once the polymerase is bound to its dsRNA substrate, nucleotide addition can be represented by a series of events which include three basic steps: NTP binding, conformational change and catalysis, and PPi release (Scheme 1).

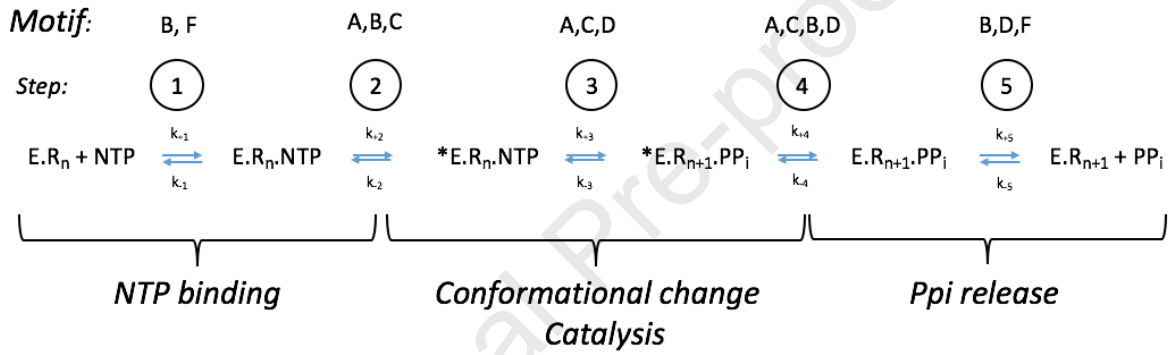


*Scheme 1. Representation of the kinetic pathway of NTP (or NA-TP) incorporation into RNA.*

Unraveling the detailed involvement of the different RdRp motifs in these reactions schemes represents a worthwhile challenge, because it would aid designing better NAs as well as understanding how mutations could confer drug-resistance.

Figure 7 show the comparative models of the HCV, DENV2, and SARS-CoV-2 RdRps in complex with the primer RNA poised for the nucleophilic attack of the primer 3'-OH on the nucleotide α-phosphate. Although HCV and DENV belong to the same *Flaviviridae* family and their RdRps share a significant homology at the amino-acid level, Fig. 7 panel A shows that there are significant differences in conserved motifs involved in nucleotide checking and fidelity.

In (Potisopon et al., 2017), we concentrated in differences of the appropriate closure of Motif A being next to the 2' position of the ribose of the incoming nucleotide. Here we want to add as an obvious difference that HCV NS5b does not have a classic Motif D (Selisko et al., 2018), which is typified by a single K689 and K798 in DENV NS5 and SARS-CoV-2 nsp12 (Fig. 7, panel A and B). Note that HCV NS5b has 2 positively charged amino acids Motif A residues R222 and H223 located in the vicinity of the γ-phosphate of the incoming NTP, whose position is only inferred in panel A, since the crystallized incoming nucleotide is the diphosphate form of sofosbuvir (SOF-DP, panel A). DENV1 to 4 NS5 contain at these positions conserved residues Ala and Gly (Potisopon et al., 2017). Interestingly, HCV is also different from both DENV and SARS-CoV-2 RdRps, in that it carries R48 that does not seem to have any equivalent in either DENV nor in SARS-CoV-2 RdRps. R48 is close to the β-phosphate of the NTP substrate, which is the phosphate adjacent to the cleaved bond generating the leaving pyrophosphate (Fig. 7 panel

A). We also note that the SARS-CoV-2 RdRp is somehow unique in this spatial region, since its Motif F containing residues K551 and R553 forms a peculiar loop unique here to SARS-CoV-2 nsp12, but present also in other CoVs and large RNA genome virus RdRps (Campagnola et al., 2022; Ferron et al., 2021).

Note that the amino acid differences in these otherwise conserved motifs reported in Figure 7 do not concern recognition of the 2'-OH by Motif B, which contains the same amino acids at structurally conserved positions in all three viral RdRps (residues S282, T287 and N291 in the case of HCV NS5b, (Appleby et al., 2015)).

Active site closure is considered to be a main check point of the correctness of the nucleotide substrate. It involves a movement of Motif A towards Motif C (Gong and Peersen, 2010), as well as closure of Motif D lysine onto the leaving pyrophosphate (Yang et al., 2012). Therefore, we surmise that the better SOF-TP incorporation by the HCV RdRp relative to other RdRps is likely due to Motif A and its pseudo-Motif D: in HCV NS5b, the pseudo-Motif D allows catalysis and passing over its fidelity checkpoint for SOF-TP, whereas for DENV NS5 and SARS-CoV-2 nsp12, Motifs A and D (there, in fact, mainly its typical lysine) do not validate the fidelity check for SOF-TP, which would correspond to step 3 in Scheme 1. In contrast, Motifs A and D of DENV1 to 4 NS5 and SARS-CoV-2 nsp12, validate the incorporation of AT-9010 where base pairing seems to allow a better accommodation of the NA even better than AT-9002.

## Discussion

The in vitro activities of AT-281 against all four DENV serotypes reported herein using Huh-7 cells infected with reporter viruses ($EC_{50}$ of 0.3-0.75 µM) are consistent with the previously reported $EC_{50}$ values for AT-281 against DENV-2 and -3 (Good et al., 2021a) using Huh-7, BHK-21 and human peripheral blood mononuclear cells infected with unmodified viral strains ($EC_{50}$ of 0.0.48-1.1 µM). Although most transformed cells are incapable of forming AT-9010 to any appreciable extent, these three cell types, as well as all primary mammalian cells and tissues investigated in vitro and in vivo can efficiently activate AT-281 and/or its diastereomer AT-511 to the active triphosphate metabolite (data on file). Additionally, the lack of cytotoxicity of AT-281 was established in these previous assays with 50% cytotoxicity values exceeding the highest concentrations tested (>85 µM in PBMCs and >170 µM in Huh-7 and BHK-21 cells).

We have determined the mechanism of action of AT-752 through the study of the interaction of its GTP analogue AT-9010 with the most conserved flavivirus enzyme, NS5. This protein a bi-functional enzyme expressing an RNA MTase at its N-terminus ~30 KDa domain, and an RNA-dependent RNA polymerase at its C-terminus ~70 KDa domain.

The MTase activity is also bi-functional, as the said domain is able to perform both an RNA cap N7-guanine methylation as well as a 2'-O methylation on the first transcribed nucleotide, a strictly conserved adenosine in the flavivirus genus. Remarkably, AT-9010 is able to selectively inhibit methylation at the 2'-OH but not at the N7-guanine. This selectivity is in line with crystal structures obtained with various RNA and cofactor substrates: If one considers that the SAM donor binding mode is identical for both methylation reactions, the GTP/RNA cap binding site would prevent binding of RNA cap substrates, whereas the N7-guanine poised for methylation supposedly would not overlap with the cap binding site.

We solved the crystal structure of AT-9010 in complex with the DENV3 MTase. It reveals that AT-9010 binds to the GTP/cap binding site in a similar manner as GTP, and its 2'-fluoro, 2'-methyl groups do not clash with any amino acid side chains. We note that the 2'-F removes a positive interaction with a Lys14, accounting for a ~10-fold better inhibition power of AT-9002. The contribution of AT-9010 binding on the MTase cap-binding site to the inhibition of viral replication in infected cells remains to be measured. Indeed, reverse genetics studies have shown that inhibition of 2'-O-MTase activity -independently of N7 MTase activity of NS5- attenuates viral replication in infected cell cultures (Chang et al., 2016). Nevertheless, if the inhibition is limited to the 2'-O-MTase activity we can expect that viral RNA lacking a cap-1 structure will be efficiently detected by the RIG-like receptor RIG-I contributing to an antiviral response involving type -1 interferon secretion . (Daffis et al., 2010). Moreover, it is also possible that the presence of the AT9010 molecule in the cap-binding site of the MTase could affect the capping activity. This possibility was not addressed in this work. If AT-9010 corrupts or inhibits viral RNA capping, we expect that this compound would induce a strong antiviral effect as the incorrectly capped viral RNAs are barely translated into viral proteins. Finally, it should also be noted that even with the modest $IC_{50}$ observed for the MTase, AT-9010 reaches high µM concentration in cells (Good et al., 2020) and could indeed participate to the inhibitor efficiency. Likewise, other steps downstream of the capping reaction might also be altered indeed, such as the co-associated conformational changes and cross-talks between the MTase and RdRp domains (El Sahili and Lescar, 2017; van den Elsen et al., 2021).

In the *Flaviviridae* family, the polymerase activity has been shown to catalyze two kinetically distinct reactions: first, a primer is assembled from ATP and GTP to form the initiating pppApG

dinucleotide (Selisko et al., 2012). This reaction is distributive and requires high concentrations of both nucleotides. Then, as NS5 binds to specific RNA structures (Lee et al., 2021), pppApG is elongated in a processive manner to synthesize full-length genomes of antigenome RNAs (Ackermann and Padmanabhan, 2001). We show that primer synthesis is barely inhibited by AT-9010, suggesting that the active site adopts a more stringent conformation disfavoring the incorporation of AT-9010 into the dinucleotide primer. However, this discrimination decreases significantly when the RdRp enters in its elongation mode. Overall, AT-9010 becomes discriminated over GTP about 14-fold, which should translate into a significant chain-termination effect given that AT-9010 reaches intracellular concentration in the same range as GTP (Good et al., 2020).

Notably, we also observed differences in overall RdRp activity across the four DENV seroptypes, as well as for Zika virus RdRp (not shown), that we interprete being due to serotype - specific sequence requirements for optimal binding to primer/template systems. However, we find discrimination values in the same order of magnitude 7- to 14-fold irrespective of the method used to measure GTP preference, *ie.*, single incorporation or multiple incorporations. The absence of difference between these two methods suggests that pyrophosphorolysis (the reversal of the polymerisation reaction shown in Scheme 1) of the chain-terminating analogue during multiple NTP addition does not occur significantly.

Intriguingly, in the +1 primer extension assay AT-9002 appears to be a 40-fold less efficient substrate than GTP, and 4-fold lower than AT-9010. In the presence of a 2'-C-methyl, the presence of a 2'-OH appears to decrease its substrate properties compared to 2'-F, suggesting that a peculiar, unexpected nucleotide conformation specific to AT-9002 is responsible for its decreased incorporation at the RdRp active site, but not its binding to the MTase active site.

2'-C-methyl GTP (AT-9002) and 2'-C-methyl ATP have been evaluated in enzyme assays by others (Lu et al., 2020). Also, 7-deaza 2'-C-methyl adenosine has shown interesting antiviral properties against flaviviruses, but its clinical evaluation was stopped due to toxicity issues (Arnold et al., 2012). Since bemnifosbuvir nor AT-752 do not show significant toxicity, the modified base or the 2'-F, or both, play a key role in evading toxicity issues when compared to the natural 2'-OH of AT-9002. It remains of great interest in the drug-design field to determine if the observed toxicity is due to the purine base or the 2'-OH of these analogues.

Last, although sofosbuvir 5'-triphosphate shares with AT-9010 the same modified ribose structure, the former is much less efficiently incorporated in RNA than the latter by both DENV and SARS-CoV-2 RdRp ((Shannon et al., 2022), and this work), indicating that a subtle structural difference of both RdRps with the HCV NS5b active site is responsible for this enhanced sofosbuvir 5'-triphosphate discrimination. A serine in Motif B (S282 in HCV) has been proposed to play a central role in checking the NTP 2'-OH prior to incorporation (Appleby et al., 2015). However, the Motif B tetrad (T287, S282, D225, N291 in the case of HCV NS5b, (Appleby et al., 2015) is conserved in all three RdRps studied here. Boehr et al. (Boehr et al., 2019) have proposed that, in poliovirus RdRp, this spatially equivalent serine might not be interfering in the initial NTP binding, but during closure of the active site upon binding of the next NTP because of steric hindrance due to the 2'-C-methyl group. This proposition was confirmed in the SARS-CoV-2 polymerase structure determined in complex with RNA and AT-9010 (Boehr et al., 2019). We thus propose that the present increased discrimination of SOF-TP observed here in DENV and SARS-CoV-2 active sites is due to the Motif D fidelity check-point, which could be more stringent in the case of these latter enzymes carrying a Motif D lysine. Then, to explain the difference between AT-9010 and SOF-TP efficiency in both DENV and SARS-CoV-2 RdRps, we propose

that the superior stacking of the purine relative to the pyrimidine base in the active site of RdRps contributes to the selection process, overcoming AT-9010 Motif D fidelity check enough to yield significant RNA chain-termination. In line with these results, bemnifosbuvir is 10-fold more potent than sofosbuvir in HCV infected cells (Good et al., 2020), and sofosbuvir does not reach a low $EC_{50}$ in DENV or SARS-CoV2 infected cells when compared to HCV infected cells ((Chen et al., 2015) and references therein).

In conclusion, AT-752 shows a mechanism of action consistent with its use as an anti-dengue drug. It would be of interest, given the NS5 conservation across the *Flavivirus* genus, to evaluate it further against other emerging viruses such as *eg*., Kyasanur forest and Omsk viruses (BSL-4 agents), or Tick-Borne Encephalitis virus.

**Acknowledgements**

The authors acknowledge SOLEIL for provision of synchrotron radiation facilities and we would like to thank beamline teams of Proxima-1 and Proxima-2 for their assistance during data collection.

**Competing interests:** S.G., K.L., A.M. and J.P.S. are employees of ATEA Pharmaceuticals, Inc. The other authors declare no competing interests.

**Funding**

This work was supported by grants from the Fondation pour la Recherche Medicale (Aide aux Equipes), and from ATEA Pharmaceuticals. MF and PSO received a post-doctoral fellowship as part of the grant from ATEA Pharmaceuticals. A part of the work was performed on the Aix-Marseille University Antiviral Drug-Design Platform (www.afmb.univ-mrs.fr/facility/plateforme-de-criblage-marseille-luminy/), and benefited from the Agence Nationale pour la Recherche through the French Infrastructure for Integrated Structural Biology (FRISBI) [ANR-10-INSB-05-01].

## References


Ackermann, M., Padmanabhan, R., 2001. De novo synthesis of RNA by the dengue virus RNA-dependent RNA polymerase exhibits temperature dependence at the initiation but not elongation phase. J. Biol. Chem. 276, 39926–39937. https://doi.org/10.1074/jbc.M104248200

Adams, P.D., Afonine, P.V., Bunkóczi, G., Chen, V.B., Davis, I.W., Echols, N., Headd, J.J., Hung, L.-W., Kapral, G.J., Grosse-Kunstleve, R.W., McCoy, A.J., Moriarty, N.W., Oeffner, R., Read, R.J., Richardson, D.C., Richardson, J.S., Terwilliger, T.C., Zwart, P.H., 2010. *PHENIX* : a comprehensive Python-based system for macromolecular structure solution. Acta Crystallogr D Biol Crystallogr 66, 213–221. https://doi.org/10.1107/S0907444909052925

Appleby, T.C., Perry, J.K., Murakami, E., Barauskas, O., Feng, J., Cho, A., Fox, D., Wetmore, D.R., McGrath, M.E., Ray, A.S., Sofia, M.J., Swaminathan, S., Edwards, T.E., 2015. Viral replication. Structural basis for RNA replication by the hepatitis C virus polymerase. Science 347, 771–775. https://doi.org/10.1126/science.1259210

Arnold, J.J., Sharma, S.D., Feng, J.Y., Ray, A.S., Smidansky, E.D., Kireeva, M.L., Cho, A., Perry, J., Vela, J.E., Park, Y., Xu, Y., Tian, Y., Babusis, D., Barauskus, O., Peterson, B.R., Gnatt, A., Kashlev, M., Zhong, W., Cameron, C.E., 2012. Sensitivity of mitochondrial transcription and resistance of RNA polymerase II dependent nuclear transcription to antiviral ribonucleosides. PLoS Pathog 8, e1003030. https://doi.org/10.1371/journal.ppat.1003030

Baker, C., Liu, Y., Zou, J., Muruato, A., Xie, X., Shi, P.-Y., 2020a. Identifying optimal capsid duplication length for the stability of reporter flaviviruses. Emerging Microbes & Infections 9, 2256–2265. https://doi.org/10.1080/22221751.2020.1829994

Baker, C., Xie, X., Zou, J., Muruato, A., Fink, K., Shi, P.-Y., 2020b. Using recombination-dependent lethal mutations to stabilize reporter flaviviruses for rapid serodiagnosis and drug discovery. EBioMedicine 57, 102838. https://doi.org/10.1016/j.ebiom.2020.102838

Barral, K., Sallamand, C., Petzold, C., Coutard, B., Collet, A., Thillier, Y., Zimmermann, J., Vasseur, J.-J., Canard, B., Rohayem, J., Debart, F., Decroly, E., 2013. Development of specific dengue virus 2'-O- and N7-methyltransferase assays for antiviral drug screening. Antiviral Res. 99, 292–300. https://doi.org/10.1016/j.antiviral.2013.06.001

Benarroch, D., Selisko, B., Locatelli, G.A., Maga, G., Romette, J.-L., Canard, B., 2004. The RNA helicase, nucleotide 5'-triphosphatase, and RNA 5'-triphosphatase activities of Dengue virus protein NS3 are Mg2+-dependent and require a functional Walker B motif in the helicase catalytic core. Virology 328, 208–218. https://doi.org/10.1016/j.virol.2004.07.004

Boehr, A.K., Arnold, J.J., Oh, H.S., Cameron, C.E., Boehr, D.D., 2019. 2'-C-methylated nucleotides terminate virus RNA synthesis by preventing active site closure of the viral RNA-dependent RNA polymerase. J Biol Chem 294, 16897–16907. https://doi.org/10.1074/jbc.RA119.010214

Campagnola, G., Govindarajan, V., Pelletier, A., Canard, B., Peersen, O.B., 2022. The SARS-CoV nsp12 Polymerase Active Site Is Tuned for Large-Genome Replication. J Virol 96, e0067122. https://doi.org/10.1128/jvi.00671-22

Chang, D.C., Hoang, L.T., Mohamed Naim, A.N., Dong, H., Schreiber, M.J., Hibberd, M.L., Tan, M.J.A., Shi, P.-Y., 2016. Evasion of early innate immune response by 2'-O-methylation of

dengue genomic RNA. Virology 499, 259–266. https://doi.org/10.1016/j.virol.2016.09.022

Chen, V.B., Arendall, W.B., Headd, J.J., Keedy, D.A., Immormino, R.M., Kapral, G.J., Murray, L.W., Richardson, J.S., Richardson, D.C., 2010. *MolProbity* : all-atom structure validation for macromolecular crystallography. Acta Crystallogr D Biol Crystallogr 66, 12–21. https://doi.org/10.1107/S0907444909042073

Chen, Y.-L., Yokokawa, F., Shi, P.-Y., 2015. The search for nucleoside/nucleotide analog inhibitors of dengue virus. Antiviral Res 122, 12–19. https://doi.org/10.1016/j.antiviral.2015.07.010

Daffis, S., Szretter, K.J., Schriewer, J., Li, J., Youn, S., Errett, J., Lin, T.-Y., Schneller, S., Zust, R., Dong, H., Thiel, V., Sen, G.C., Fensterl, V., Klimstra, W.B., Pierson, T.C., Buller, R.M., Gale, M., Shi, P.-Y., Diamond, M.S., 2010. 2'-O methylation of the viral mRNA cap evades host restriction by IFIT family members. Nature 468, 452–456. https://doi.org/10.1038/nature09489

Doughty, C.T., Yawetz, S., Lyons, J., 2017. Emerging Causes of Arbovirus Encephalitis in North America: Powassan, Chikungunya, and Zika Viruses. Curr Neurol Neurosci Rep 17, 12. https://doi.org/10.1007/s11910-017-0724-3

Dousson, C.B., 2018. Current and future use of nucleo(s)tide prodrugs in the treatment of hepatitis C virus infection. Antivir Chem Chemother 26, 2040206618756430. https://doi.org/10.1177/2040206618756430

Egloff, M.-P., Benarroch, D., Selisko, B., Romette, J.-L., Canard, B., 2002. An RNA cap (nucleoside-2'-O-)-methyltransferase in the flavivirus RNA polymerase NS5: crystal structure and functional characterization. EMBO J. 21, 2757–2768. https://doi.org/10.1093/emboj/21.11.2757

El Sahili, A., Lescar, J., 2017. Dengue Virus Non-Structural Protein 5. Viruses 9, E91. https://doi.org/10.3390/v9040091

Emsley, P., Cowtan, K., 2004. *Coot* : model-building tools for molecular graphics. Acta Crystallogr D Biol Crystallogr 60, 2126–2132. https://doi.org/10.1107/S0907444904019158

Ferron, F., Sama, B., Decroly, E., Canard, B., 2021. The enzymes for genome size increase and maintenance of large (+)RNA viruses. Trends Biochem Sci 46, 866–877. https://doi.org/10.1016/j.tibs.2021.05.006

Filomatori, C.V., Iglesias, N.G., Villordo, S.M., Alvarez, D.E., Gamarnik, A.V., 2011. RNA sequences and structures required for the recruitment and activity of the dengue virus polymerase. J. Biol. Chem. 286, 6929–6939. https://doi.org/10.1074/jbc.M110.162289

Ghetia, C., Bhatt, P., Mukhopadhyay, C., 2022. Association of dengue virus non-structural-1 protein with disease severity: a brief review. Trans R Soc Trop Med Hyg trac087. https://doi.org/10.1093/trstmh/trac087

Gong, P., Peersen, O.B., 2010. Structural basis for active site closure by the poliovirus RNA-dependent RNA polymerase. Proc. Natl. Acad. Sci. U.S.A. 107, 22505–22510. https://doi.org/10.1073/pnas.1007626107

Good, S.S., Moussa, A., Zhou, X.-J., Pietropaolo, K., Sommadossi, J.-P., 2020. Preclinical evaluation of AT-527, a novel guanosine nucleotide prodrug with potent, pan-genotypic activity against hepatitis C virus. PLoS One 15, e0227104. https://doi.org/10.1371/journal.pone.0227104

Good, S.S., Shannon, A., Lin, K., Moussa, A., Julander, J.G., La Colla, P., Collu, G., Canard, B., Sommadossi, J.-P., 2021a. Evaluation of AT-752, a Double Prodrug of a Guanosine Nucleotide Analog with In Vitro and In Vivo Activity against Dengue and Other Flaviviruses. Antimicrob Agents Chemother 65, e0098821. https://doi.org/10.1128/AAC.00988-21

Good, S.S., Westover, J., Jung, K.H., Zhou, X.-J., Moussa, A., La Colla, P., Collu, G., Canard, B., Sommadossi, J.-P., 2021b. AT-527, a double prodrug of a guanosine nucleotide analog, is a potent inhibitor of SARS-CoV-2 in vitro and a promising oral antiviral for treatment of COVID-19. Antimicrob Agents Chemother. https://doi.org/10.1128/AAC.02479-20

Kaptein, S.J.F., Goethals, O., Kiemel, D., Marchand, A., Kesteleyn, B., Bonfanti, J.-F., Bardiot, D., Stoops, B., Jonckers, T.H.M., Dallmeier, K., Geluykens, P., Thys, K., Crabbe, M., Chatel-Chaix, L., Münster, M., Querat, G., Touret, F., de Lamballerie, X., Raboisson, P., Simmen, K., Chaltin, P., Bartenschlager, R., Van Loock, M., Neyts, J., 2021. A pan-serotype dengue virus inhibitor targeting the NS3-NS4B interaction. Nature 598, 504–509. https://doi.org/10.1038/s41586-021-03990-6

Kuczera, D., Assolini, J.P., Tomiotto-Pellissier, F., Pavanelli, W.R., Silveira, G.F., 2018. Highlights for Dengue Immunopathogenesis: Antibody-Dependent Enhancement, Cytokine Storm, and Beyond. J. Interferon Cytokine Res. 38, 69–80. https://doi.org/10.1089/jir.2017.0037

Lantez, V., Dalle, K., Charrel, R., Baronti, C., Canard, B., Coutard, B., 2011. Comparative Production Analysis of Three Phlebovirus Nucleoproteins under Denaturing or Non-Denaturing Conditions for Crystallographic Studies. PLoS Negl Trop Dis 5, e936. https://doi.org/10.1371/journal.pntd.0000936

Lee, E., Bujalowski, P.J., Teramoto, T., Gottipati, K., Scott, S.D., Padmanabhan, R., Choi, K.H., 2021. Structures of flavivirus RNA promoters suggest two binding modes with NS5 polymerase. Nat Commun 12, 2530. https://doi.org/10.1038/s41467-021-22846-1

Lim, S.P., Noble, C.G., Shi, P.-Y., 2015. The dengue virus NS5 protein as a target for drug discovery. Antiviral Res. 119, 57–67. https://doi.org/10.1016/j.antiviral.2015.04.010

Lim, S.P., Sonntag, L.S., Noble, C., Nilar, S.H., Ng, R.H., Zou, G., Monaghan, P., Chung, K.Y., Dong, H., Liu, B., Bodenreider, C., Lee, G., Ding, M., Chan, W.L., Wang, G., Jian, Y.L., Chao, A.T., Lescar, J., Yin, Z., Vedananda, T.R., Keller, T.H., Shi, P.-Y., 2011. Small molecule inhibitors that selectively block dengue virus methyltransferase. J. Biol. Chem. 286, 6233–6240. https://doi.org/10.1074/jbc.M110.179184

Lin, K., Good, S.S., Julander, J.G., Weight, A.E., Moussa, A., Sommadossi, J.-P., 2022. AT-752, a double prodrug of a guanosine nucleotide analog, inhibits yellow fever virus in a hamster model. PLoS Negl Trop Dis 16, e0009937. https://doi.org/10.1371/journal.pntd.0009937

Lu, G., Zhang, X., Zheng, W., Sun, J., Hua, L., Xu, L., Chu, X.-J., Ding, S., Xiong, W., 2020. Development of a Simple In Vitro Assay To Identify and Evaluate Nucleotide Analogs against SARS-CoV-2 RNA-Dependent RNA Polymerase. Antimicrob Agents Chemother 65, e01508-20. https://doi.org/10.1128/AAC.01508-20

Masmejan, S., Musso, D., Vouga, M., Pomar, L., Dashraath, P., Stojanov, M., Panchaud, A., Baud, D., 2020. Zika Virus. Pathogens 9, E898. https://doi.org/10.3390/pathogens9110898

McCoy, A.J., Grosse-Kunstleve, R.W., Adams, P.D., Winn, M.D., Storoni, L.C., Read, R.J., 2007. *Phaser* crystallographic software. J Appl Crystallogr 40, 658–674. https://doi.org/10.1107/S0021889807021206

Moquin, S.A., Simon, O., Karuna, R., Lakshminarayana, S.B., Yokokawa, F., Wang, F., Saravanan, C., Zhang, J., Day, C.W., Chan, K., Wang, Q.-Y., Lu, S., Dong, H., Wan, K.F., Lim, S.P., Liu, W., Seh, C.C., Chen, Y.-L., Xu, H., Barkan, D.T., Kounde, C.S., Sim, W.L.S., Wang, G., Yeo, H.-Q., Zou, B., Chan, W.L., Ding, M., Song, J.-G., Li, M., Osborne, C., Blasco, F., Sarko, C., Beer, D., Bonamy, G.M.C., Sasseville, V.G., Shi, P.-Y., Diagana, T.T., Yeung, B.K.S., Gu, F., 2021. NITD-688, a pan-serotype inhibitor of the dengue virus NS4B protein, shows favorable pharmacokinetics and efficacy in preclinical animal models. Sci. Transl. Med. 13, eabb2181. https://doi.org/10.1126/scitranslmed.abb2181

Murakami, E., Wang, T., Babusis, D., Lepist, E.-I., Sauer, D., Park, Y., Vela, J.E., Shih, R., Birkus, G., Stefanidis, D., Kim, C.U., Cho, A., Ray, A.S., 2014. Metabolism and pharmacokinetics of the anti-hepatitis C virus nucleotide prodrug GS-6620. Antimicrob Agents Chemother 58, 1943–1951. https://doi.org/10.1128/AAC.02350-13

Paesen, G.C., Collet, A., Sallamand, C., Debart, F., Vasseur, J.-J., Canard, B., Decroly, E., Grimes, J.M., 2015. X-ray structure and activities of an essential Mononegavirales L-protein domain. Nat Commun 6, 8749. https://doi.org/10.1038/ncomms9749

Peersen, O.B., 2019. A Comprehensive Superposition of Viral Polymerase Structures. Viruses 11. https://doi.org/10.3390/v11080745

Pettersen, E.F., Goddard, T.D., Huang, C.C., Couch, G.S., Greenblatt, D.M., Meng, E.C., Ferrin, T.E., 2004. UCSF Chimera--a visualization system for exploratory research and analysis. J Comput Chem 25, 1605–1612. https://doi.org/10.1002/jcc.20084

Pierson, T.C., Diamond, M.S., 2020. The continued threat of emerging flaviviruses. Nat Microbiol 5, 796–812. https://doi.org/10.1038/s41564-020-0714-0

Potisopon S, Ferron F, Fattorini V, Selisko B, Canard B. 2017. Substrate selectivity of Dengue and Zika virus NS5 polymerase towards 2'-modified nucleotide analogues. Antiviral Res. 2017 Apr;140:25-36. doi: 10.1016/j.antiviral.2016.12.021.

Ramanathan, A., Robb, G.B., Chan, S.-H., 2016. mRNA capping: biological functions and applications. Nucleic Acids Res. 44, 7511–7526. https://doi.org/10.1093/nar/gkw551

Ray, D., Shah, A., Tilgner, M., Guo, Y., Zhao, Y., Dong, H., Deas, T.S., Zhou, Y., Li, H., Shi, P.-Y., 2006. West Nile virus 5'-cap structure is formed by sequential guanine N-7 and ribose 2'-O methylations by nonstructural protein 5. J. Virol. 80, 8362–8370. https://doi.org/10.1128/JVI.00814-06

Rivera, L., Biswal, S., Sáez-Llorens, X., Reynales, H., López-Medina, E., Borja-Tabora, C., Bravo, L., Sirivichayakul, C., Kosalaraksa, P., Martinez Vargas, L., Yu, D., Watanaveeradej, V., Espinoza, F., Dietze, R., Fernando, L., Wickramasinghe, P., Duarte MoreiraJr, E., Fernando, A.D., Gunasekera, D., Luz, K., Venâncioda Cunha, R., Rauscher, M., Zent, O., Liu, M., Hoffman, E., LeFevre, I., Tricou, V., Wallace, D., Alera, M., Borkowski, A., 2022. Three-year Efficacy and Safety of Takeda's Dengue Vaccine Candidate (TAK-003). Clinical Infectious Diseases 75, 107–117. https://doi.org/10.1093/cid/ciab864

Selisko, B., Dutartre, H., Guillemot, J.-C., Debarnot, C., Benarroch, D., Khromykh, A., Desprès, P., Egloff, M.-P., Canard, B., 2006. Comparative mechanistic studies of de novo RNA synthesis by flavivirus RNA-dependent RNA polymerases. Virology 351, 145–158. https://doi.org/10.1016/j.virol.2006.03.026

Selisko, B., Papageorgiou, N., Ferron, F., Canard, B., 2018. Structural and Functional Basis of the Fidelity of Nucleotide Selection by Flavivirus RNA-Dependent RNA Polymerases. Viruses 10. https://doi.org/10.3390/v10020059

Selisko, B., Potisopon, S., Agred, R., Priet, S., Varlet, I., Thillier, Y., Sallamand, C., Debart, F., Vasseur, J.-J., Canard, B., 2012. Molecular basis for nucleotide conservation at the ends of the dengue virus genome. PLoS Pathog. 8, e1002912. https://doi.org/10.1371/journal.ppat.1002912

Shannon, A., Fattorini, V., Sama, B., Selisko, B., Feracci, M., Falcou, C., Gauffre, P., El Kazzi, P., Delpal, A., Decroly, E., Alvarez, K., Eydoux, C., Guillemot, J.-C., Moussa, A., Good, S.S., La Colla, P., Lin, K., Sommadossi, J.-P., Zhu, Y., Yan, X., Shi, H., Ferron, F., Canard, B., 2022. A dual mechanism of action of AT-527 against SARS-CoV-2 polymerase. Nature Communications 13, 621. https://doi.org/10.1038/s41467-022-28113-1

Shannon, A., Selisko, B., Le, N.-T.-T., Huchting, J., Touret, F., Piorkowski, G., Fattorini, V., Ferron, F., Decroly, E., Meier, C., Coutard, B., Peersen, O., Canard, B., 2020. Rapid incorporation of Favipiravir by the fast and permissive viral RNA polymerase complex results in SARS-CoV-2 lethal mutagenesis. Nat Commun 11, 4682. https://doi.org/10.1038/s41467-020-18463-z

van den Elsen, K., Quek, J.P., Luo, D., 2021. Molecular Insights into the Flavivirus Replication Complex. Viruses 13, 956. https://doi.org/10.3390/v13060956

Vonrhein, C., Flensburg, C., Keller, P., Sharff, A., Smart, O., Paciorek, W., Womack, T., Bricogne, G., 2011. Data processing and analysis with the *autoPROC* toolbox. Acta Crystallogr D Biol Crystallogr 67, 293–302. https://doi.org/10.1107/S0907444911007773

Wang, Y., Xie, X., Shi, P.-Y., 2022. Flavivirus NS4B protein: Structure, function, and antiviral discovery. Antiviral Research 207, 105423. https://doi.org/10.1016/j.antiviral.2022.105423

Yang, X., Smidansky, E.D., Maksimchuk, K.R., Lum, D., Welch, J.L., Arnold, J.J., Cameron, C.E., Boehr, D.D., 2012. Motif D of viral RNA-dependent RNA polymerases determines efficiency and fidelity of nucleotide addition. Structure 20, 1519–1527. https://doi.org/10.1016/j.str.2012.06.012

## Material and methods

### 5'-triphosphate nucleosides, dinucleotide synthesis, and nucleic acid sequences

AT-9010, 5'-triphosphate 2'-fluoro-2'-C-methyl uridine, and Remdesivir 5'-triphosphate were from NuBlocks LLC, Oceanside, CA, USA. Other NTPs were purchased from GE Healthcare. Chemical synthesis of 5'-triphosphate (TP) dinucleotides pppUpU, pppUpG, pppGpU and pppApU was performed on an ABI 394 synthesizer (Applied Biosystems) and purified as described in (Shannon et al., 2020). The accession numbers of NS5 sequences used here are available at www.ncbi.nlm.nih.gov under the following accession numbers: DENV1_NS5: NP_722465; DENV2_NS5: NP_739590; DENV3_NS5: YP_001531176; DENV4_NS5: NP_740325 .

### Antiviral assays

Transcripts of the dengue viruses (DENV1 WP, DENV2 NGC, DENV3 VN32, DENV4 MY01) were modified with a nano luciferase reporter between the 5'UTR and capsid gene as previously described (Baker et al., 2020b, 2020a) to create tagged viruses that are stable with cell culture passaging while producing a robust luciferase signal after inoculation for efficient screening of antiviral activity. Eight 2-fold serial dilutions of AT-281 were mixed with each reporter virus (MOIs of 0.1 for DENV1, DENV2 and DENV3; MOI of 0.001 for DENV4) and added to plates containing Huh-7 cells (RRID: CVCL 0336) that were seeded at $1 \times 10^4$ cells per well in a 96-well plate the previous day in Dulbecco's Modified Eagle Medium (Invitrogen, Carlsbad, CA) with 2% fetal bovine serum (Hyclone, Logan, UT). Cells were washed 48 h post infection three times with phosphate-buffered saline, followed by addition of NanoGlo® substrate diluted 1:100 in NanoGlo® Assay Buffer (Promega, Madison, WI). Luciferase activities were read by a BioTek Cytation 5 plate reader after 3 minutes. Data were analyzed with GraphPad Prism 9 software. Luciferase activities were normalized to DMSO treatment samples which were set to 100%. Error bars represent mean ± SD. Results are representative of three independent experiments with each one analyzed in triplicate.

### Expression of DENV NS5, RdRp and MTase domains

Full length DENV NS5 and RdRp domains used in this study were expressed under the control of a T7-promoter in pET28a vectors in Escherichia coli (*E. coli*) NEB C2566 cells (New England Biolabs) carrying the pRARE2LacI (Novagen) plasmid. Proteins were expressed overnight at 17°C in TB (with 25 µg/ml Kanamycin and 17 µg/ml Chloramphenicol), following induction with 100 µM IPTG at an $OD_{600nm}$ of 0.8 – 1. EtOH was added to 2% (v/v) final concentration.
DENV MTases were expressed under the control of a T7-promoter in pDEST17 vectors in Escherichia coli (*E. coli*) ) NEB C2566 cells (New England Biolabs) carrying the pRARE2LacI (Novagen) plasmid. Proteins were expressed overnight at 17°C in TB (with 100 µg/mL Ampicillin and 17 µg/mL Chloramphenicol), following induction with 200 µM IPTG at an $OD_{600nm}$ of 0.8 – 1. EtOH was added to 2% (v/v) final concentration.

### Purification of DENV NS5

The cells were disrupted by sonication on ice in a lysis buffer (50 mM NaP pH 8, 1 M NaCl, 20% glycerol) supplemented with, 1.0 mg/mL Lysozyme, 22 µg/mL DNase, 1.6 % igepal, 0.5 mM TCEP and a complete protease inhibitor cocktail (COC) from Roche. Protein from the soluble fraction was loaded onto TALON® Superflow™ cobalt-based IMAC resin (Cytiva), washed 5 times with lysis buffer, 10 times with lysis buffer (igepal free) prior to elution with a lysis buffer supplemented with 250 mM imidazole and 250 mM glycine. Imidazole was removed by an overnight dialysis in a dialysis buffer (50 mM NaP pH 8, 20 % glycerol, 150 mM NaCl, 250 mM glycine and 0.5 mM TCEP) before to perform a last step purification using a size exclusion chromatography (SEC) HiLoad® 16/600 Superdex® 200 pg column in a buffer (10 mM HEPES pH 8, 300 mM NaCl, 10% glycerol and 0.5 mM TCEP). Protein was then concentrated to 10 to 15 $mg.mL^{-1}$ and stored at -80°C after a last dialysis in the SEC buffer supplemented with 40 % of glycerol.

**Purification of DENV RdRp domains**

The cells were disrupted by sonication on ice in a lysis buffer (50 mM NaP pH 8, 1 M NaCl, 20% glycerol) supplemented with, 1.0 mg/mL Lysozyme, 22 µg/mL DNase, 1.6 % igepal, 0.5 mM TCEP and a complete protease inhibitor cocktail (COC) from Roche. Protein from the soluble fraction were loaded onto TALON® Superflow™ cobalt-based IMAC resin (Cytiva), washed 5 times with lysis buffer, 10 times with lysis buffer (igepal free) prior to elution with a lysis buffer supplemented with 250 mM imidazole and 250 mM glycine. Imidazole was removed by an overnight dialysis in a dialysis buffer (50 mM NaP pH 8, 20 % glycerol, 150 mM NaCl, 250 mM glycine and 0.5 mM TCEP) before to perform a last step purification using a GE Hi-trap Heparine column. Protein was then concentrated to 10 to 15 $mg.mL^{-1}$ and stored at -80°C after a last dialysis in a final buffer containing 20 mM HEPES pH 8, 300 mM NaCl, 40 % of glycerol and 0.5 mM TCEP.

**Purification of DENV MTase domains**

The cells were disrupted by sonication on ice in a lysis buffer (50mM HEPES pH 7.5, 10 % glycerol, 500 mM NaCl and 5 mM Imidazole) supplemented with 0.2 mM Benzamidine, 1 mg/mL Lysozyme, 22 µg/mL DNase and 0.5 mM TCEP. Protein from the soluble fraction were loaded onto TALON® Superflow™ cobalt-based IMAC resin (Cytiva) and washed with lysis buffer (1M NaCl) prior to elution with 250 mM imidazole. The protein was finally purified with a SEC (HiLoad® 16/600 Superdex® 200 pg) in a buffer of 50 mM HEPES pH 8, 300 mM NaCl and 0.5 mM TCEP. Protein was then concentrated to 10 to 15 $mg.mL^{-1}$ and stored at -80°C after a last dialysis in a final buffer containing 20 mM HEPES pH 8, 300 mM NaCl, 40 % of glycerol and 0.5 mM TCEP.

**Thermal shift assay**

The thermal stability of the DENV1 to 4 proteins and their interaction with compounds were evaluated by using a thermal shift assay. Reactions were performed in white frame star PCR 96-well plates (Greiner ref 044705) with a final volume of 20 µl. The best conditions were found by using a 20 mM HEPES buffer, pH 7.5 containing 50 mM NaCl, 5 mM DTT, 10% glycerol and 1M Sorbitol.

Volumes of 0.4 µl of GTP, sinefungin or AT-9010 were disposed in the plate (100 µM final concentration). Water was used as a control without compound. 2 µM of NS5, 2 µM of RdRp domains or 6µM of MTase domains were mixed in the buffer with 2.5X, 0.75X or 1.5X of dye, respectively (final concentrations). The mix of protein and Protein thermal shift kit from ThermoFisher (ref 4461146) was prepared and 19.6 µl were dispensed into each well. The plate was sealed with adhesive film and then submitted to a run on a CFX96 RT-PCR (Bio-Rad). The program started by a 1-min equilibration phase at 20°C, followed by a temperature gradient of 0.5°C/30 s, from 20°C to 95°C, recording fluorescence every 0.5°C. Fluorescence was recorded using the FRET channel. Every experiment was performed in triplicate. Curves were plotted and analyzed to determine the melting temperature $T_m$ by using the Boltzmann sigmoidal equation with the GraphPad Prism software.

**pppApG Primer synthesis**

Reactions were done in 50 mM HEPES buffer, pH 8.0 containing 10 mM KCl, 10 mM DTT and 10 µM template 5'-AACAGGUUCU-3' (corresponding to the 3' end of the DENV2 genome), 1 µM DENV2 NS5, 100 µM non-labeled NTPs and increasing concentrations of AT-9010, and either 5 mM $MgCl_2$ or 2 mM $MnCl_2$, as given in the Figure. Radiolabeled [$\gamma$-$^{32}$P]-ATP was used at 0.3 µCi per µl reaction volume (3000 Ci/mmol, Hartmann Analytics). Reactions were started by addition of a mixture of NTPs and catalytic ions. At given time points samples were taken, reactions stopped by adding an equal volume of FBD stop solution (formamide, 10 mM EDTA). Reaction products were separated using sequencing gels of 20% acrylamide-bisacrylamide (19:1), 7 M urea with TTE buffer (89 mM Tris pH 8.0, 28 mM taurine (2-aminoethanesulfonic acid), 0.5 mM EDTA). RNA product bands were visualized using an Amersham™ Typhoon™ Biomolecular Imager (Cytiva). The intensity of each band was quantified using the ImageQuant software (Cytiva). For $IC_{50}$ measurements, values were normalized and fitted with Prism (GraphPad software) using the following equation: Y=100/(1+((X/$IC_{50}$)^Hillslope)). $IC_{50}$ is defined as the inhibitory compound concentration that causes 50 % reduction in enzyme activity. Reactions were done either four times (Mn) or twice (Mg), independently.

**MTase activity assay**

The transfer of tritiated methyl from [$^3$H]-SAM onto RNA substrate was monitored by filter-binding assay (FBA), performed according to the method described previously (Paesen et al., 2015). The recombinant methyltransferase domain of the non- structural protein NS5 from DENV serotype 2 (DENV NS5 MTase) corresponding to residues 1–296 of NS5 was expressed and purified as described previously (Egloff et al., 2002). FBA was carried out in reaction mixture [40 mM Tris-HCl (pH 8.0), 1 mM DTT, 2 µM SAM and 0.1 µM 3H-SAM (Perkin Elmer)] in the presence of 0.7 µM $^m$GpppAC4 synthetic RNA and DENV2 NS5MTase protein (500 nM). The enzyme was first mixed with the compound (.5 to 1000 µM) suspended in water before the addition of RNA substrate and SAM and then incubated at 30°C. Reaction mixtures were stopped after 30 min by their 10-fold dilution in ice-cold water. Samples were transferred to diethylaminoethyl (DEAE) filtermat (Perkin Elmer) using a Filtermat Harvester (Packard Instruments). The RNA-retaining mats were washed twice with 10 mM ammonium formate pH 8.0, twice with water and once with ethanol. They were soaked with scintillation fluid (Perkin Elmer), and $^3$H-methyl transfer to the RNA substrates was determined using a Wallac MicroBeta TriLux Liquid

Scintillation Counter (Perkin Elmer). For $IC_{50}$ measurements, values were normalized and fitted with Prism (GraphPad software) using the following equation: Y=100/(1+((X/$IC_{50}$)^Hillslope)). $IC_{50}$ is defined as the inhibitory compound concentration that causes 50 % reduction in enzyme activity.

**Incorporation of nucleotide analogues into RNA**

DENV NS5 proteins were pre-incubated with the annealed $P_{10}/T_{20}$ RNA (either the DENV2-specific combination to test multiple NTP incorporations: 6Fam-5'-AGUUGUUAGU-3'/5'-GUCCACGUAGACUAACAACU-3', or the non-specific combinations to study single nucleotide incorporations: Cy5-5'-GUCAUUCUCC-3'/5'-UAGCUUCUUAGGAGAAUG-3' AC for U incorporation or Cy5-5'-GUCAUUCUCC-3'/5'-UAGCUUCUUCGGAGAAUGAC-3' for G incorporation) in an assembly buffer containing 20 mM HEPES pH 7.5, 10% glycerol, 5 mM $MgCl_2$, and 5 mM DTT for 10 min at 30°C to create an active RNA elongation complex.
Multiple nucleotide incorporation was tested as follows. Reactions were started by adding AT-9010 with either all four NTPs or UTP, ATP, and CTP only. Final concentrations were 1 μM DENV NS5, 0.25 μM $P_{10}/T_{20}$, 100 μM of each NTP, and between 10 and 625 μM AT-9010 in a final buffer containing 20 mM HEPES pH 7.5, 15% glycerol, 5 mM $MgCl_2$, and 5 mM DTT.
Single nucleotide incorporation was tested as follows. Reactions were started by adding the corresponding NTP or analogue. Final concentrations were 1 μM NS5, 0.25 μM $P_{10}/T_{20}$, 100 μM NTP or analogue in a final buffer containing 20 mM HEPES pH 7.5, 15% glycerol, 5 mM $MgCl_2$, and 5 mM DTT. Reactions were quenched at designated time points in 3× volume FBD stop solution (formamide, 10 mM EDTA) and products were separated using sequencing gels of 20% acrylamide-bisacrylamide (19:1), 7 M urea with TBE buffer. RNA product bands were visualized using an Amersham™ Typhoon™ Biomolecular Imager (Cytiva). The intensity of each band was quantified using the ImageQuant software (Cytiva).

**Crystallographic and modeling studies**

The construct used for crystallization was the same as described in (Barral et al., 2013) with a cleavable Hexahistidine-Thioredoxin tag at the N-terminus of DENV3 NS5 coding sequence (amino acids region 1-277) in plasmid pMcox20A. Transformed E. coli T7 express cells (New England BioLabs) were grown at 37°C in LB medium supplemented with 100μg/mL ampicillin, to an $OD_{600nm}$ of 0.6-0.8. Expression of the recombinant protein was induced by the addition of 100μM IPTG, and incubation was continued for a further 16h at 17°C. The cells were harvested by centrifugation at 8000g for 10 min at 4°C and stored at -80°C. The purification of the protein and the tag removal was performed in non-denaturing conditions as described in (Lantez et al., 2011) by using TALON® Superflow™ cobalt-based IMAC resin (Cytiva) for affinity chromatography. The final size exclusion chromatography step was performed using a Superdex S200 HiLoad 16/60 column with a buffer containing 20 mM HEPES pH 7.5, 200 mM NaCl, 10% glycerol and 2 mM DTT.
Crystallization conditions were adapted from (Lim et al., 2011) using the sitting-drop vapor diffusion method using crystallization buffer. All crystals were grown at 293.15 K, using a 1 : 2 ratio of protein (10 mg/mL) to precipitant solution (22% PEG 8000, 200 mM NaCl, 20 mM Tri-Sodium Citrate, 100 mM Tris pH 8.5). Crystals grew in 4 days and were soaked overnight with 1

mM of AT-9010 (final concentration). All crystals were cryo-protected with reservoir solution supplemented with 10% glycerol, and flash-frozen in liquid nitrogen at 100 K.
Data collection and diffraction data were collected at Soleil synchrotron. Original native data set was collected on Proxima2. Data set was processed and analysed with autoPROC toolbox (Vonrhein et al., 2011). Structure was solved by molecular replacement using PHASER (McCoy et al., 2007) and PDB 4CTK as a reference model. As previously observed the crystal Asymmetric Unit is composed of 2 chains, however the additional positive density blobs found in both chain is not equivalent. In one chain the extra density corresponds to a single molecule of SAM while in the other chain the positive density corresponds to one SAH and an AT-9010 molecules. The model was build using COOT (Emsley and Cowtan, 2004) and refined at 1.90 Å using PHENIX (Adams et al., 2010). The structure was checked and confirmed to have good stereochemistry according to MOLPROBITY (Chen et al., 2010). Data collection and refinement statistics are listed in Table 2. Structural analysis and figures was done using UCSF CHIMERA (Pettersen et al., 2004).

**Table 1.** Thermal shift analysis of four serotypes of DENV NS5 domains (MTase and RdRp) and full-length NS5 in the presence of GTP, the MTase inhibitor sinefungin, and the GTP analogue AT-9010.

| | $\Delta T_m$(°C) | DENV1 | DENV2 | DENV3 | DENV4 |
|---|---|---|---|---|---|
| **MTase domain** | --- | --- | --- | --- | --- |
| | GTP | 4.9 ± 0.1 | 5.7 ± 0.1 | 4.1 ± 0.1 | 4.0 ± 0.1 |
| | Sinefungin | 1.9 ± 0.1 | 2.9 ± 0.1 | 2.1 ± 0.1 | 2.8 ± 0.1 |
| | AT-9010 | 3.8 ± 0.1 | 4.0 ± 0.1 | 3.5 ± 0.1 | 2.9 ± 0.1 |
| | | | | | |
| **RdRp domain** | --- | --- | --- | --- | --- |
| | GTP | 4.5 ± 0.2 | 2.4 ± 0.1 | 2.2 ± 0.1 | 3.3 ± 0.1 |
| | Sinefungin | -0.1 ± 0.1 | -0.8 ± 0.1 | 0.0 ± 0.1 | -0.1 ± 0.1 |
| | AT-9010 | 5.6 ± 0.1 | 3.8 ± 0.1 | 3.2 ± 0.1 | 4.1 ± 0.1 |
| | | | | | |
| **NS5** | --- | --- | --- | --- | --- |
| | GTP | 5.8 ± 0.1 | 5.7 ± 0.1 | 4.8 ± 0.1 | 3.9 ± 0.1 |
| | Sinefungin | 1.2 ± 0.1 | 1.4 ± 0.1 | 1.8 ± 0.1 | 1.4 ± 0.1 |
| | AT-9010 | 6.1 ± 0.1 | 6.0 ± 0.1 | 5.0 ± 0.1 | 4.8 ± 0.1 |

**Table 2.** Crystallographic data and statistic for the DENV3 MTase/AT-9010 complex. Statistics for the highest-resolution shell are shown in parentheses.

| **Data processing** | |
|---|---|
| | **DENV3 MTase** complexed with soaked **AT-9010** |
| Wavelength (Å) | 0.9801 |
| Space group | P 21 21 2 |
| – a, b, c (Å) | 61.26, 184.13, 52.15 |
| – α, β, γ (°) | 90.00, 90.00, 90.00 |
| Resolution range (Å) | 45.38 - 1.9 (1.97 - 1.9) |
| Total No. of reflections | 583677 (27381) |
| No. of unique reflections | 45354 (2284) |
| Completeness (%) | 96.0 (97.8) |
| Multiplicity | 12.9 (12.0) |
| I/σ(I) | 18.5 (4.7) |
| R meas | 0.093 (0.46) |
| R merge | 0.089 (0.44) |
| R-pim | 0.026 (0.13) |
| CC1/2 | 0.99 (0.94) |
| Wilson B-factor (Å) | 24.6 |
| **Structure solution & refinement** | |
| No. of reflections, working set | 45347 (4551) |
| No. of reflections, test set (%) | 2195 (217), 5.0 % |
| $R_{work}$ | 0.20 (0.27) |
| $R_{free}$ | 0.24 (0.33) |
| No. of non-H atoms | 4589 |
| -Protein | 4162 |
| -Ligand | 65 |
| -Water | 362 |
| ***R.M.S. deviations*** | Protein residues 516 |
| -Bonds (Å) | 0.013 |
| -Angles (°) | 1.21 |
| Average B-factors (Å$^2$) | 29.38 |
| -Protein | 28.68 |
| -Ligand | 41.71 |
| -Water | 35.22 |
| ***Ramachandran Plot*** | |
| -Favoured (%) | 98.04 |
| -Allowed (%) | 1.96 |
| -Outliers (%) | 0.00 |
| Clashcore | 5.21 |
| **PDB code** | 8BCR |

**Table 3.** Preference for GTP over AT-9010, AT-9002, and of UTP over SOF-TP for the four serotypes of DENV NS5 in a single nucleotide incorporation assay. Incorporation rates ($R_{NTP}$) of individual 5'-triphosphate analogues were determined as described in 'Material and Methods', and preference for GTP over AT-9010 or AT-9002 and UTP over SOF-TP is reported as $P = R_{GTP}/R_{AT\text{-}9010}$, $P = R_{GTP}/R_{AT\text{-}9002}$, $P = R_{UTP}/R_{SOF\text{-}TP}$.

| Preference | DENV1 | DENV2 | DENV3 | DENV4 |
|---|---|---|---|---|
| **GTP > AT-9010** | 7.7 ± 0.5 | 9.3 ± 0.1 | 11.6 ± 1.3 | 11.2 ± 0.7 |
| **GTP > AT-9002** | 19.4 ± 2.8 | 18.2 ± 0.2 | 17.5 ± 1.5 | 41.5 ± 7.3 |
| **UTP > SOF-TP** | > 100 | > 100 | > 100 | > 100 |

**Table 4.** Conservation and identification of essential amino acids in contact with the phosphates of the incoming nucleotide in viral RdRps HCV NS5b, DENV2 NS5, and SARS-CoV2 nsp12. The Protein Data Bank (PDB, www.rcsb.org/) codes used are 4WTG for HCV, 5ZQK for DENV2, and 7ED5 for SARS-CoV-2 nsp12.

| Virus<br><br>Contacts at | HCV | DENV2 | SARS-CoV-2 |
|---|---|---|---|
| α- phosphate | R158 | R472 | R555 |
| β- phosphate | R48 | - | R553* |
| γ- phosphate | K51, R222, H223 | K358 | K551* |
| Motif D residue | - | K689 | K798 |
| Other features | H223 corresponds to SARS Motif D K621 | - | K551 and R553 CoV unique Motif F<br>K621 corresponds to HCV H223 |

**Figure legends**

**Figure 1.** Cartoon representing the flavivirus NS5 bi-functional MTase and RdRp enzyme, with potentially inhibited enzyme activities. The NS5 protein is represented from N- to C-terminus, with the conserved sequence motifs A-to-G reported along NS5. Structures of the two guanosine analogues AT-9010 and AT-9002 along with sofosbuvir-5'-triphosphate studied here are represented below the NS5 protein, together with relevant enzyme activities.

**Figure 2.** *In vitro* activity of AT-281 against DENV1–4 reporters. Serial dilutions of AT-281 and virus modified with a nano luciferase reporter (MOIs of 0.1 for DENV1, DENV2 and DENV3; MOI of 0.001 for DENV4) were added to 96-well plates seeded with $1x10^4$ Huh-7 cells per well. After incubation for 48 h, cells were washed and $EC_{50}$ values were determined by luciferase activities. Data were normalized to DMSO treatment samples which were set to 100%. Error bars represent mean ± SD. Results are representative of three independent experiments with each one analyzed in triplicate

**Figure 3.** Thermal stability shift experiments showing the stabilizing effect of GTP, AT-9010 or Sinefungin on the DENV serotype 1 to 4 MTases, RdRp and NS5 protein. The values are reported in delta Tm (ΔTm (°C)) using the proteins alone as a baseline.

**Figure 4. Functional and structural basis of inhibition of the DENV MTase by AT-9010.** A) Dose-response determination using a filter binding assay (FBA). Reactions were incubated at 30°C during 30 min and the enzymatic activity was determined using FBA as described in the Material and Methods section.
B) Overall structure of DENV3 MTase represented in blue ribbons complexed with SAH and AT-9010 represented as sticks. AT-9010 is located at the Cap binding site. C) Omit map at 1σ of the AT-9010. D) Close view of the AT-9010 binding in the GTP binding site. Interacting residues are labelled and shown as sticks. E) Structural comparison of the position of a GTP (pink) and AT9010 (light brown) bound in the Cap binding site. Cap binding site structures belong to DENV2 (in pink - PDB 2P1D)) and DENV3 (in light brown) MTases and are conserved.

**Figure 5. AT-9010 incorporation and inhibition during *de novo* initiation reaction by DENV2 NS5.**
A) PAGE analysis of *de novo* initiation reactions using a 10-nt template corresponding to the 3' end of the genome (AACAGGUUCU) resulting in the formation of pppApG, pppApGpA and pppApGpApA over time. GTP was either replaced by AT9010 or AT9010 was added in increasing concentrations to the reactions containing 100 µM GTP. B) Inhibition of *de novo* product formation by AT-9010 based on the quantification of product bands of four (Mn) or two (Mg) independent reactions; the corresponding $IC_{50}$ values are given.

**Figure 6. Discrimination of AT-9010, AT-9002, and SOF-TP by DENV4 NS5 against their natural nucleotide competitors GTP, GTP, and UTP, respectively.** A) Primer extension assay allowing multiple insertion of ATP, CTP, and UTP in the absence, the presence of GTP; or the presence of a mixture of GTP and AT-9010 as indicated below the auto-fluorograph of the gel. The nature of regular inserted Watson-Crick nucleotides is indicated in the right of the gel. B) Primer extension assay allowing incorporation of a single nucleotide GTP, AT-9010, AT-9002,

UTP or SOF-TP. Quantification of band-products greater in size than the G/AT (+5) band relative to the G/AT (+5) band were measured using a Typhoon FluorImager, and allowed to calculate the discrimination value. The incorporation rates for AT-901 and AT9002 are compared to that of GTP, and to that of UTP in the case of SOF-TP. Similar results for other DENV1 - 3 NS5s are reported in Supplementary Figures 1-3.

**Figure 7. Comparison of RdRp active sites of HCV, DENV, and SARS-CoV-2 RdRps.** A) The HCV NS5b (PDB: 4WTG) was superimposed onto DENV2 NS5 (PDB: 5ZQK). Amino acid side chains in the vicinity of Motif D and as well as the nucleotide phosphates are represented. The Motif D region is represented in orange for HCV. Metal A and B are represented with purple and orange spheres in the vicinity of the Motif A and C catalytic aspartates, respectively. Unique amino acid labels discussed in the text are represented in red. B) The SARS-CoV-2 nsp12 structure (PDB:) was superimposed onto DENV NS5 (PDB: 5ZQK). The Motif D Lysine amino acid side chain is shown in red for SARS-CoV-2 nsp12 and grey for DENV NS5, respectively. Essential amino acids contacting the nucleotide phosphates are represented. A unique Metal B is represented with a green sphere in the vicinity of the Motif A and C catalytic aspartates, respectively (Shannon et al., 2022). Unique amino acid labels discussed in the text are represented in red.

**Scheme 1.** Representation of the kinetic pathway of NTP (or NA-TP) incorporation into RNA. The cartoon starts on the left with the viral RdRp bound to its RNA substrate. The main individual steps are numbered 1 to 5. The RdRp Motifs A to G involved in this scheme are indicated on top, as reported in the literature and reviewed in Selisko et al, 2018. E: enzyme; $R_n$: RNA of n nucleotides in length; PPi: inorganic pyrophosphate. *indicates an enzyme undergoing a conformational change.

## Appendix A

### Legends to supplementary Figures

**Supplementary Fig. 1.**
Primer extension assay allowing incorporation of a single nucleotide GTP, AT-9010, AT-9002, UTP, or SOF-TP as described for Fig. 6B, but reported comparatively for the 4 serotypes of DENV NS5. Measurements and quantitations were as in the legend of Fig. 6. The incorporation rates for AT-9010 and AT9002 are compared to that of GTP, and to that of UTP in the case of SOF-TP.

**Supplementary Fig. 2**
Quantification of the gels shown in Supplementary Fig. 1, and graphic representation of the incorporation rates. The incorporation rates for AT-9010 and AT9002 are compared to that of GTP, and to that of UTP in the case of SOF-TP.

**Supplementary Fig. 3**
Primer extension assay allowing incorporation of multiple nucleotide AT-9010 with either all four NTPs or UTP, ATP, and CTP only as described for Fig. 6A, but reported comparatively for the 4 serotypes of DENV NS5.

# Appendix B

## 1- Supplementary data. AT-281 Characterization

1. **$^{1}$H-NMR Spectrum;**

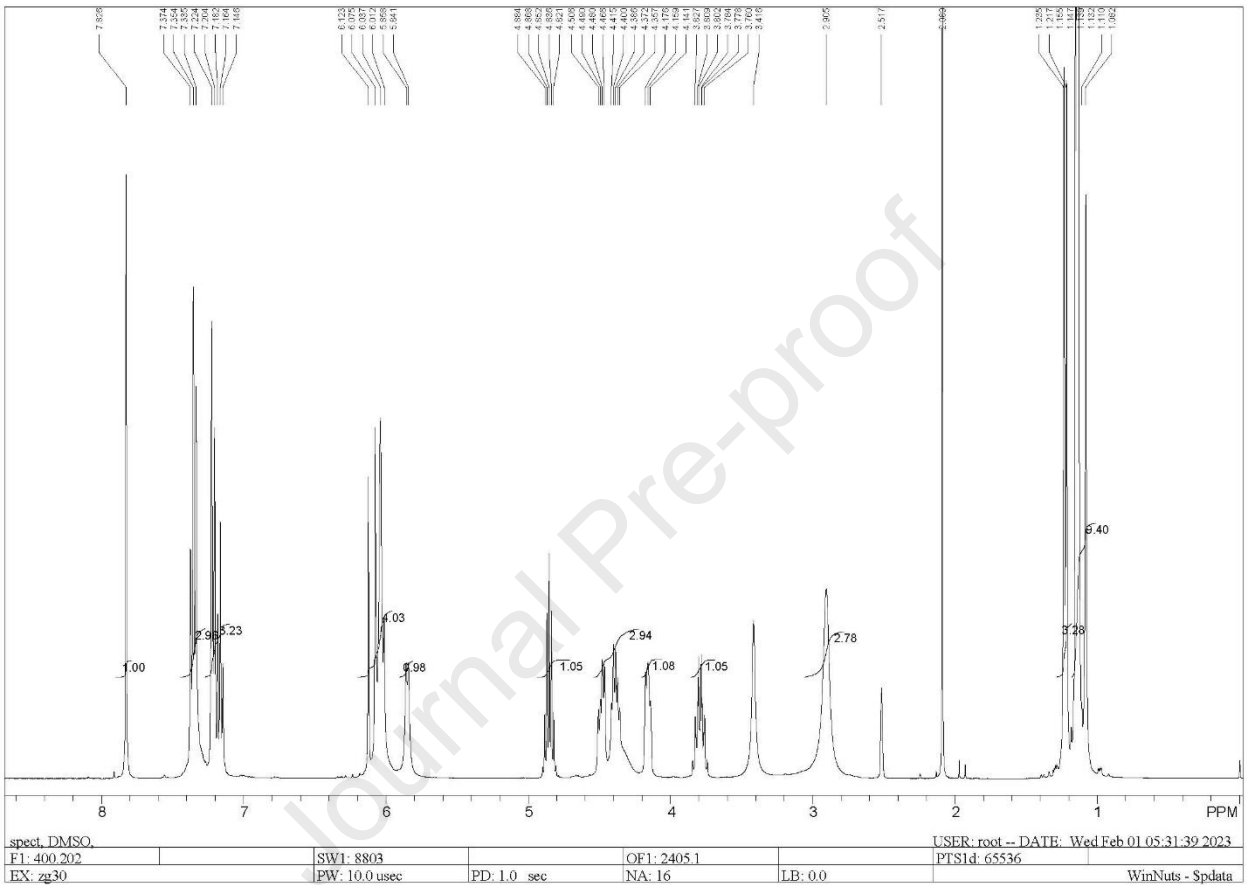


2. **$^{13}$C-NMR Spectrum**:

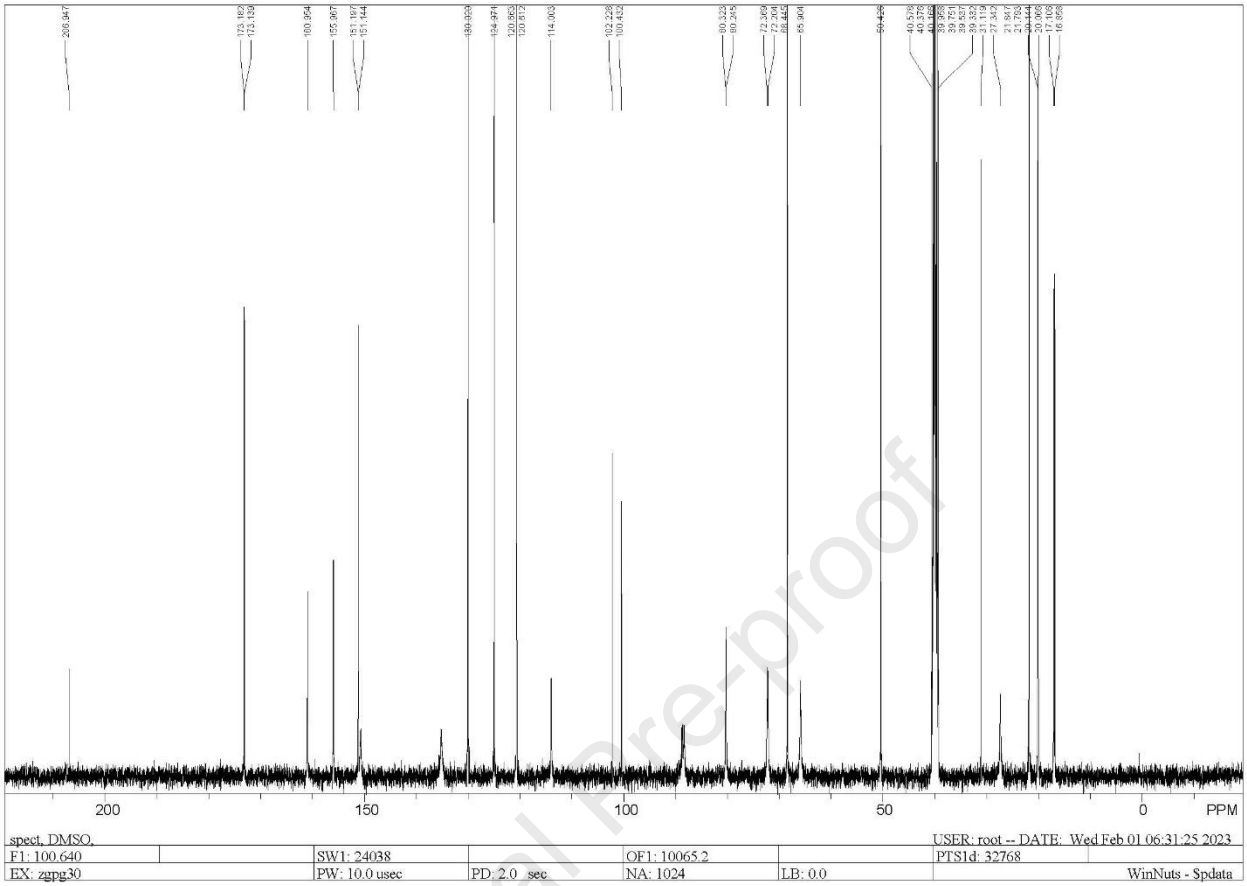


**3. MS Spectrum:**

## Library Search Summary

**Injection Details**

| | | | |
|---|---|---|---|
| *Injection Name:* | **AT-281 20032501** | *Run Time (min):* | **5.00** |
| *Vial Number:* | **BD6** | *Injection Volume:* | **5.00** |
| *Injection Type:* | **Unknown** | | |
| *Calibration Level:* | | | |
| *Instrument Method:* | **MS-ESI-pos** | | |
| *Processing Method:* | **MS Quantitative** | *Dilution Factor:* | **1.0000** |
| *Injection Date/Time:* | **27/Apr/20 16:03** | *Sample Weight:* | **1.0000** |

**Library Search Results**

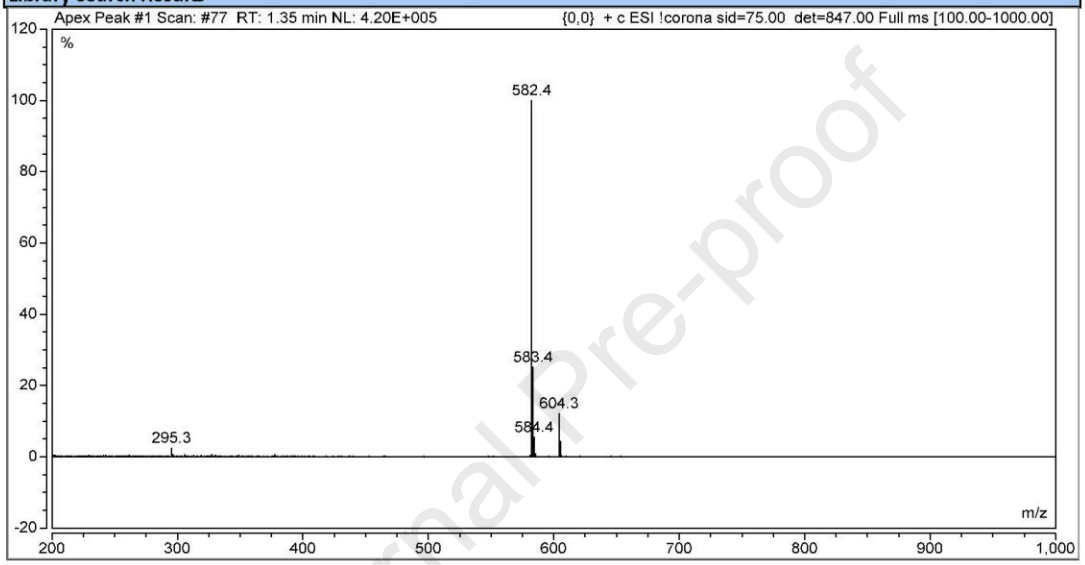






### 4. HPLC Conditions and Chromatogram:

HPLC method:

Column：Agilent ZORBAX SB-C18 5 μm 4.6 * 250 mm

Mobile phase A：10mM $KH_2PO_4$（Dissolve 1.36 g $KH_2PO_4$ in water and dilute to 1000 mL with water.）

Filter the mobile phase through 0.45μm membrane filter and degas it by ultrasound prior to use.
Mobile phase B：Acetonitrile
Gradient elution

| Time（min） | Mobile Phase A (%) | Mobile Phase B (%) |
|---|---|---|
| 0 | 90 | 10 |
| 5 | 90 | 10 |
| 15 | 30 | 70 |
| 30 | 30 | 70 |
| 30.1 | 90 | 10 |
| 40 | 90 | 10 |
| Column | 35℃ | |
| Detection | 254 nm | |
| Injection volume | 10μL | |
| Flow rate | 1.0 mL/min | |
| Diluent | Acetonitrile/Water=1/9 | |

# Chromatogram and Results

## Injection Details

| | | | |
|---|---|---|---|
| Injection Name: | AT-281_20032501 | Run Time (min): | 30.00 |
| Vial Number: | Vial:82 | Injection Volume: | 10.00 |
| Injection Type: | Unknown | Channel: | DAD_Signal_A |
| Instrument: | QC-82 | Wavelength(nm): | 254 |
| Instrument Method: | AT-527 | Operator: | yuyanjiao |
| Processing Method: | Quantitative | Processing Method Viersion: | 3 |
| Injection Date/Time: | 23/02/2022 18:03:10 | Processing Method update time: | 24/02/22 10:24:32 |

**File:** chrom://dcserver/Data_TPN/AT527/20220222-01.seq/135.smp/DAD_Signal_A.channel/DAD_Signal_A.chm

## Chromatogram

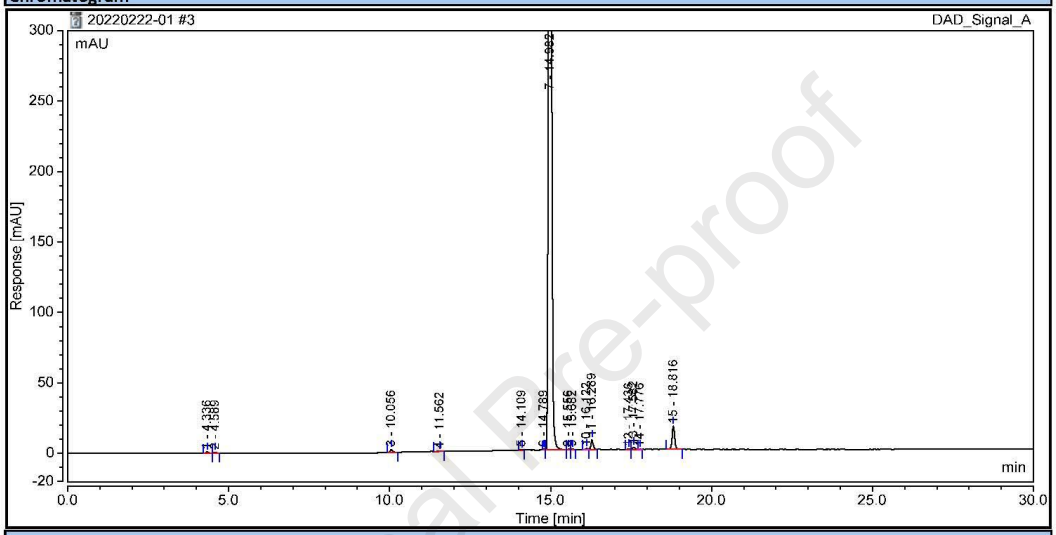


## Integration Results

| No. | Peak Name | Retention Time min | Area mAU*s | Height mAU | Relative Area % | S/N | Resolution (EP) |
|---|---|---|---|---|---|---|---|
| 1 | | 4.336 | 5.23140 | 0.898 | 0.0601 | 5.7 | 1.78 |
| 2 | | 4.589 | 4.56935 | 0.887 | 0.0525 | 5.6 | 43.06 |
| 3 | | 10.056 | 11.24457 | 2.349 | 0.1291 | 14.9 | 12.93 |
| 4 | | 11.562 | 1.71082 | 0.298 | 0.0196 | 1.9 | 24.25 |
| 5 | | 14.109 | 2.19443 | 0.618 | 0.0252 | 3.9 | 7.33 |
| 6 | | 14.789 | 1.40928 | 0.446 | 0.0162 | 2.8 | 1.83 |
| 7 | | 14.982 | 8540.14256 | 1811.868 | 98.0868 | 11531.7 | 4.07 |
| 8 | | 15.556 | 2.26454 | 0.410 | 0.0260 | 2.6 | 0.94 |
| 9 | | 15.682 | 1.91469 | 0.461 | 0.0220 | 2.9 | 5.41 |
| 10 | | 16.122 | 2.92926 | 0.759 | 0.0336 | 4.8 | n.a. |
| 11 | | 16.289 | 33.27090 | 7.262 | 0.3821 | 46.2 | 9.76 |
| 12 | | 17.436 | 1.88090 | 0.409 | 0.0216 | 2.6 | 1.19 |
| 13 | | 17.582 | 9.20000 | 1.832 | 0.1057 | 11.7 | 9.49 |
| 14 | | 17.776 | 0.91709 | 0.210 | 0.0105 | 1.3 | n.a. |
| 15 | | 18.816 | 87.84131 | 16.539 | 1.0089 | 105.3 | n.a. |
| **Total:** | | | **8706.721** | **1845.246** | **100.0000** | **11744.15** | |

## 2. Supplementary data. Synthesis of AT-752

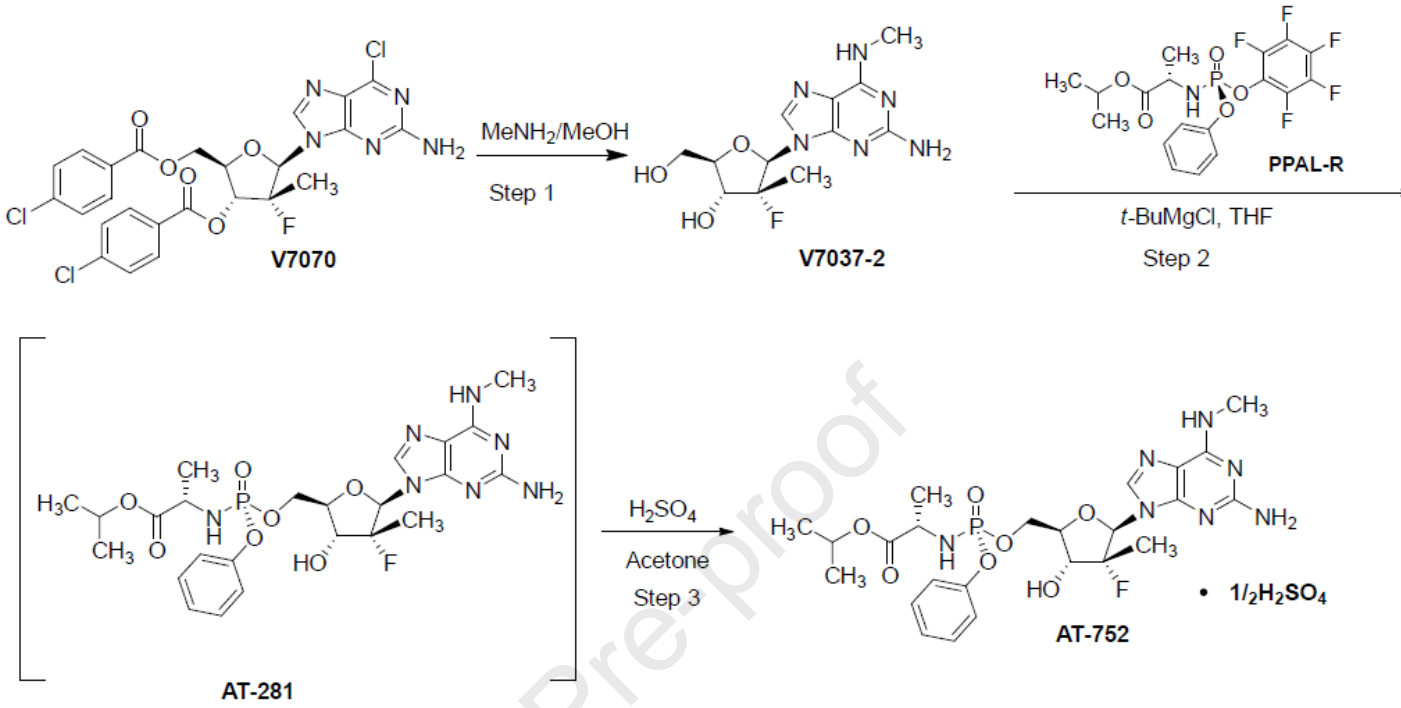


The synthesis starts with V7070. In this step, the 4-Cl-Bz-protecting groups in V7070 are fully removed and the Cl in the purine ring is displaced with methylamine in methanol to give V7037-2.
The V7037-2 is then further purified by stirring in and precipitation from anhydrous ethanol.
In Step 2, the purified V7037-2 is coupled with PPAL-R. Step 2 yields AT-281, the free base of AT-752, as a solution in acetone, which is used in the next step without isolation.
In Step 3, AT-281 is reacted with sulfuric acid in acetone to give AT-752 as an amorphous solid.
Specifications for the proposed starting materials have been established.

Reagents and Solvents:

- Step 1: V7070, methanol, methylamine gas, sodium hydroxide, anhydrous ethanol, diatomaceous earth, ethyl acetate.
- Step 2: PPAL-R, tert-butylmagnesium chloride, tetrahydrofuran, sulfuric acid, isopropyl acetate, sodium bicarbonate, dichloromethane, sodium chloride, anhydrous sodium sulphate, methyl tert-butyl ether and acetone.
- Step 3: Acetone, sulfuric acid, methyl tert-butyl ether, activated carbon.

**3. Supplementary data. Characterization of AT-752**

## 1.1. $^{1}$H-NMR AT-752

The chemical structure as determined by proton nuclear magnetic resonance spectroscopy ($^{1}$H-NMR) is provided in Figure 1. Details of the $^{1}$H-NMR results are provided in Table 1. The $^{1}$H-NMR assignments presented in Table 3 are consistent with the chemical structure of AT-752.

The $^{1}$H-NMR spectra are provided in Figure 2 (full spectrum) and Figure 3 - Figure 5 (zoom in spectra).

**Figure 1: AT-752 Elucidation of Structure Determination by $^{1}$H-NMR**

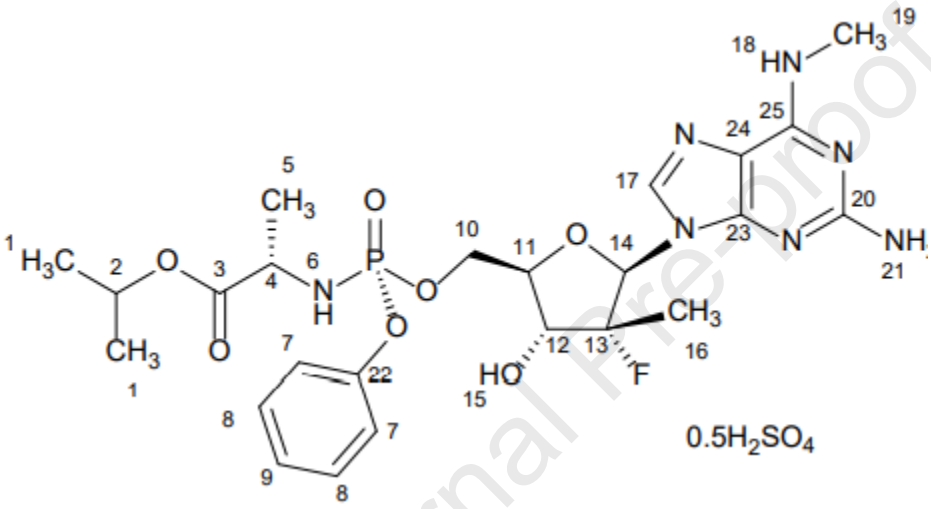

**Table 1: AT-752 Structure Elucidation – $^{1}$H-NMR Results**

| δ (ppm) | Number of H | Multiplicity | Peak assignment | Coupling constant (Hz) |
|---|---|---|---|---|
| 8.44 | 1 | br | 18-H | NA |
| 7.97 | 1 | s | 17-H | NA |
| 7.33 | 2 | m | 8-H | NA |
| 7.16 | 3 | m | 7-H, 9-H | NA |
| 6.88 | 2 | br | 21-H | NA |
| 6.10 | 1 | d | 14-H | $J_{H\text{-}F}$ = 18.87 Hz |
| 6.04 | 1 | dd | 6-H | $J_{C\text{-}H}$ = 10.62 Hz, 12.81 Hz |
| 5.91 | 1 | br | 11-H | NA |
| 4.83 | 1 | septet | 2-H | 6.20 |
| 4.42 | 3 | m | 10H, 12-H | NA |
| 4.17 | 1 | m | 15-H | NA |
| 3.77 | 1 | m | 4-H | NA |
| 3.36 | 1 | br | 0.5 $H_2SO_4$ | NA |
| 2.96 | 3 | s | 19-H | NA |
| 1.20 | 3 | d | 5-H | 7.05 |
| 1.12 | 9 | m | 1-H<br>16-H | NA |

br = broad signal; d = doublet; dd = doublet of doublets: m = multiplet; NA = not applicable; s = singlet
Note that the solvent is DMSO-*d*6

**Figure 2: AT-752 Structure Elucidation - $^{1}$H-NMR Spectrum (Full Spectrum)**

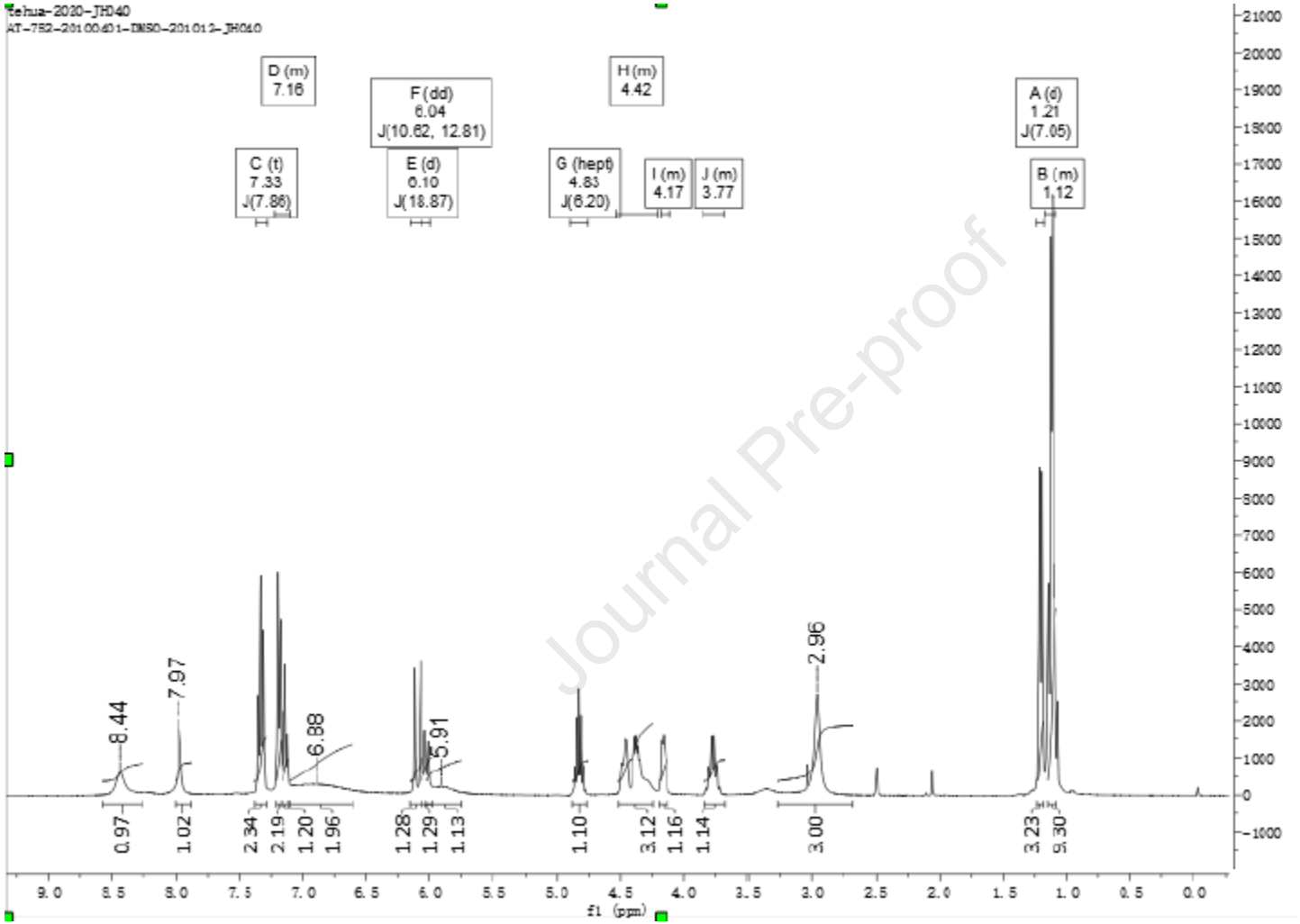

**Figure 3: AT-752 Structure Elucidation - $^{1}$H-NMR Spectrum (Zoom In)**

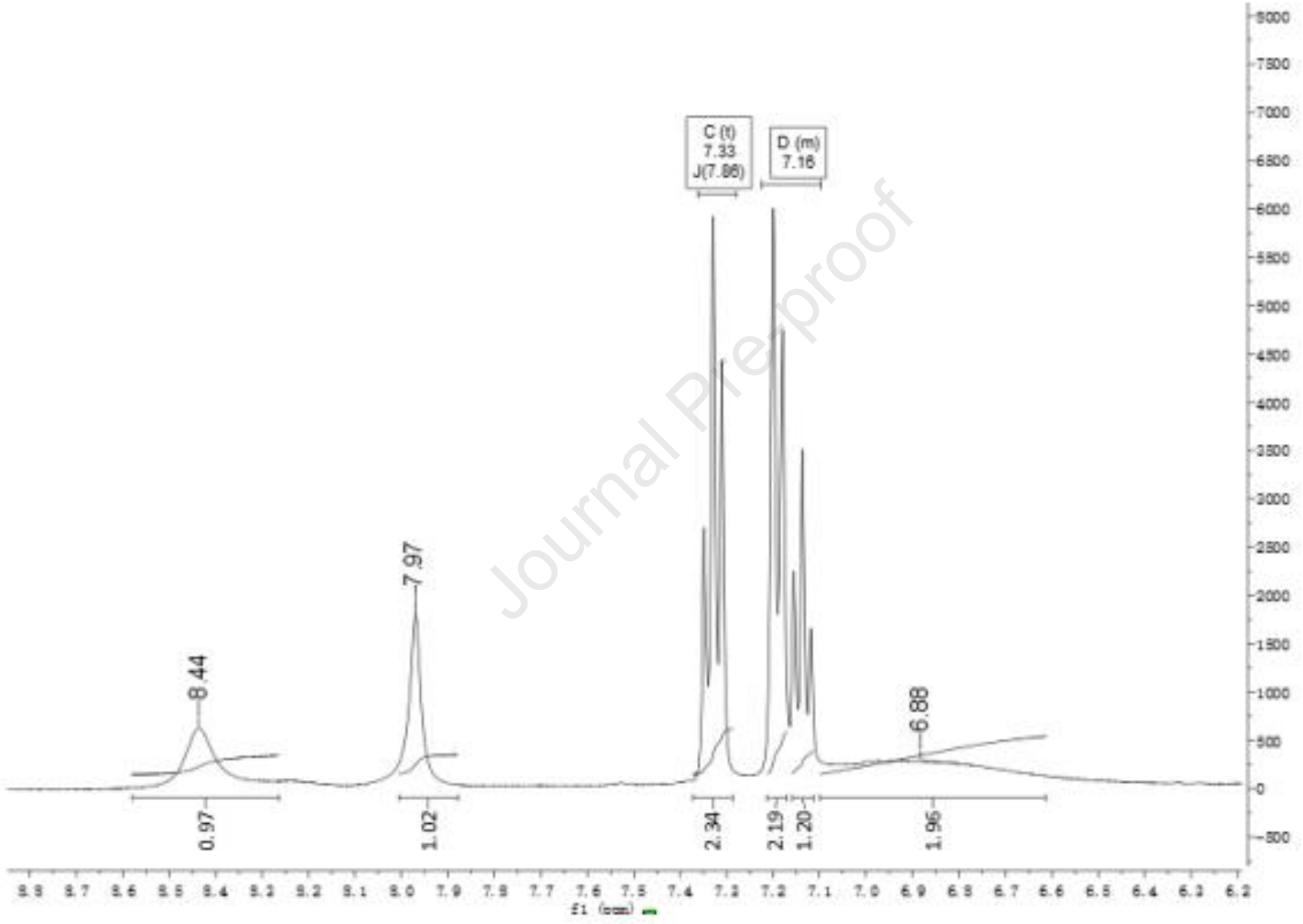

**Figure 4: AT-752 Structure Elucidation - $^{1}$H-NMR Spectrum (Zoom In, continued)**

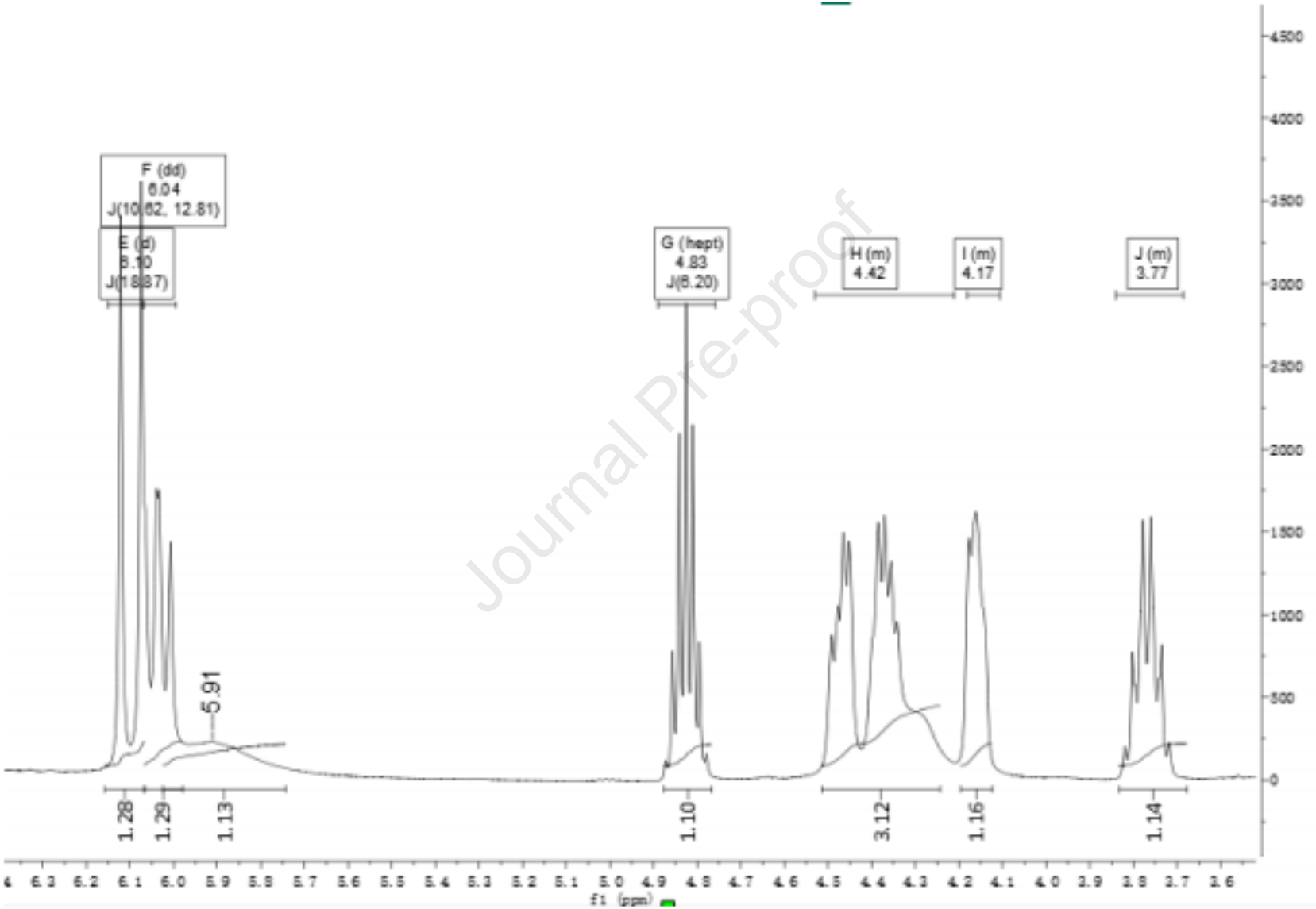

**Figure 5: AT-752 Structure Elucidation - $^{1}$H-NMR Spectrum (Zoom In, continued)**

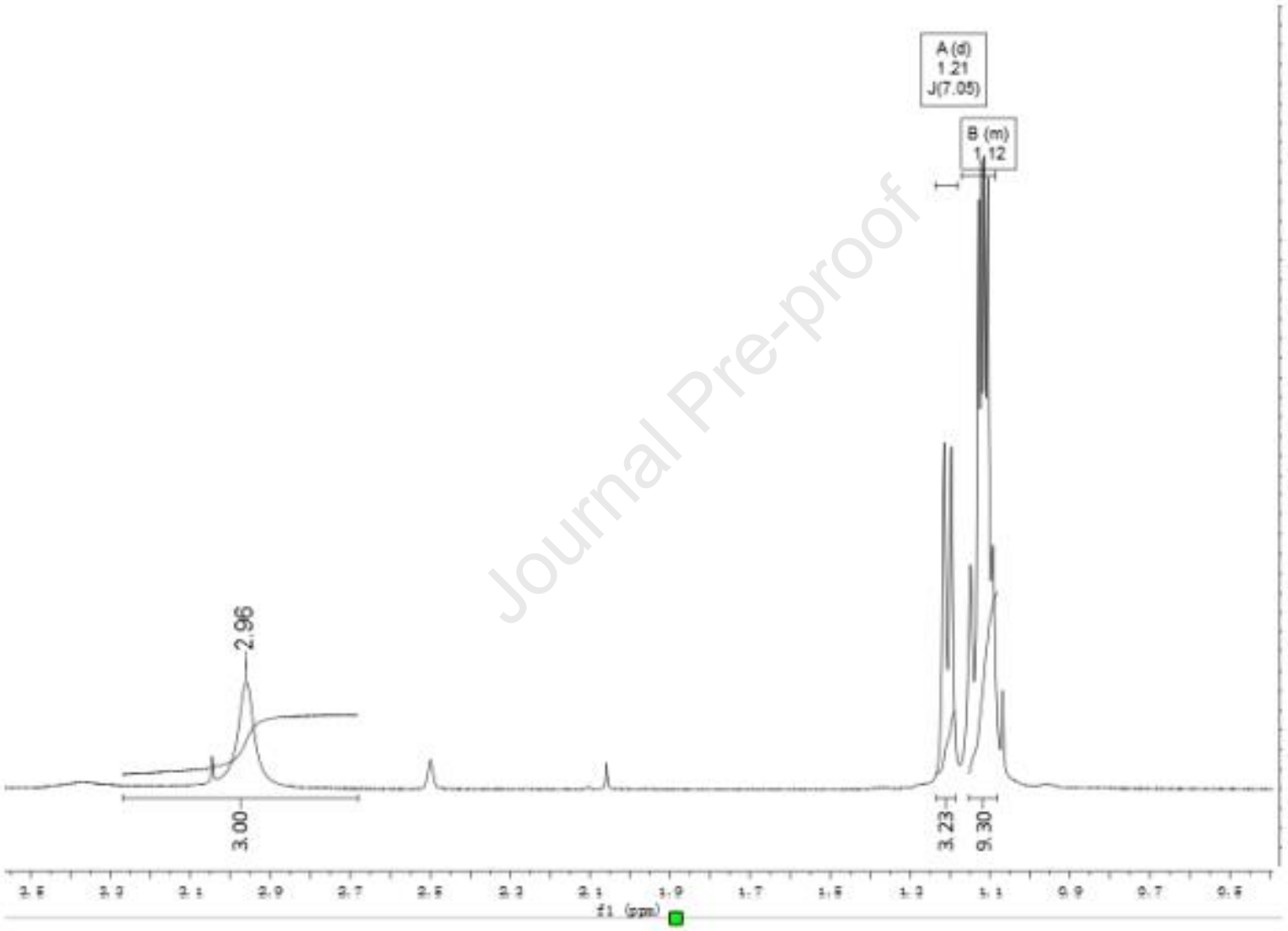

## 1.2. $^{13}$C-NMR

$^{13}$C-NMR results are shown in Table 2. Distortionless Enhancement by Polarization Transfer at 135° (DEPT--135) was also used in combination with the $^{13}$C--NMR to classify the carbon atoms in the AT-752 molecule into four types. CH and $CH_3$ carbon will show a positive phase, while $CH_2$ carbon will show a negative signal and quaternary carbon will not be observed. The DEPT--135 results are shown in **Error! Reference source not found.**, with the interpretation following the table.

The AT-752 structure is provided in Figure 6. The $^{13}$C-NMR spectra are provided in Figure 7 (full spectrum), and Figure 8 through Figure 10 (zoom in spectra), respectively.

**Figure 6: AT-752 Elucidation of Structure by $^{13}$C-NMR**

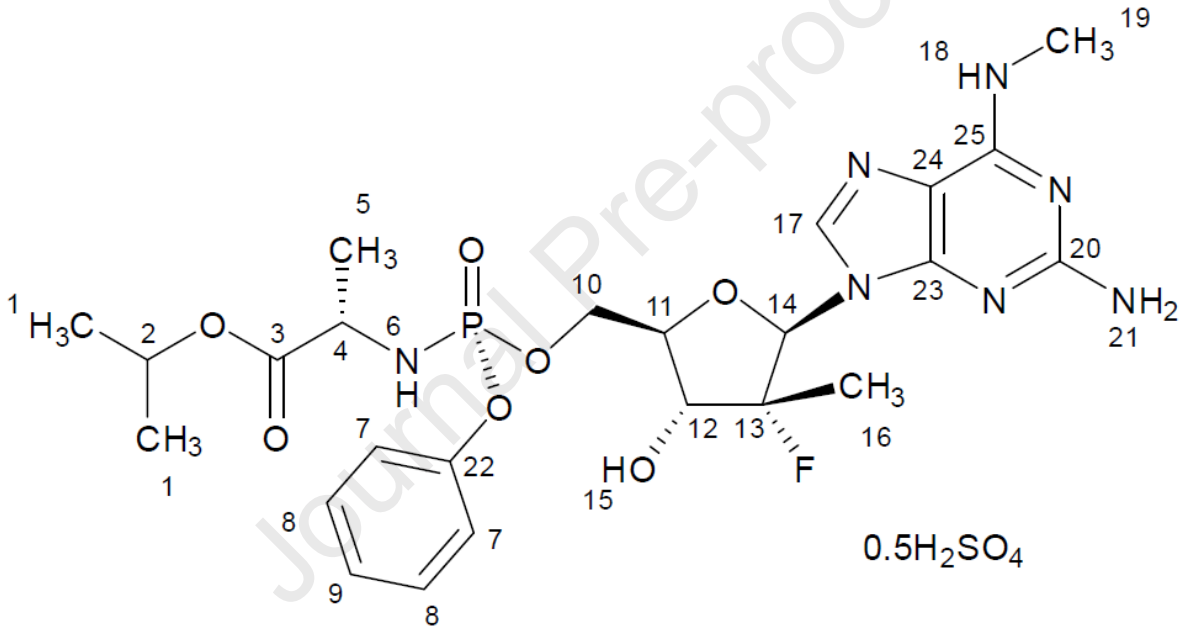

**Figure 7: AT-752 Structure Elucidation–$^{13}$C-NMR (Full Spectrum)**

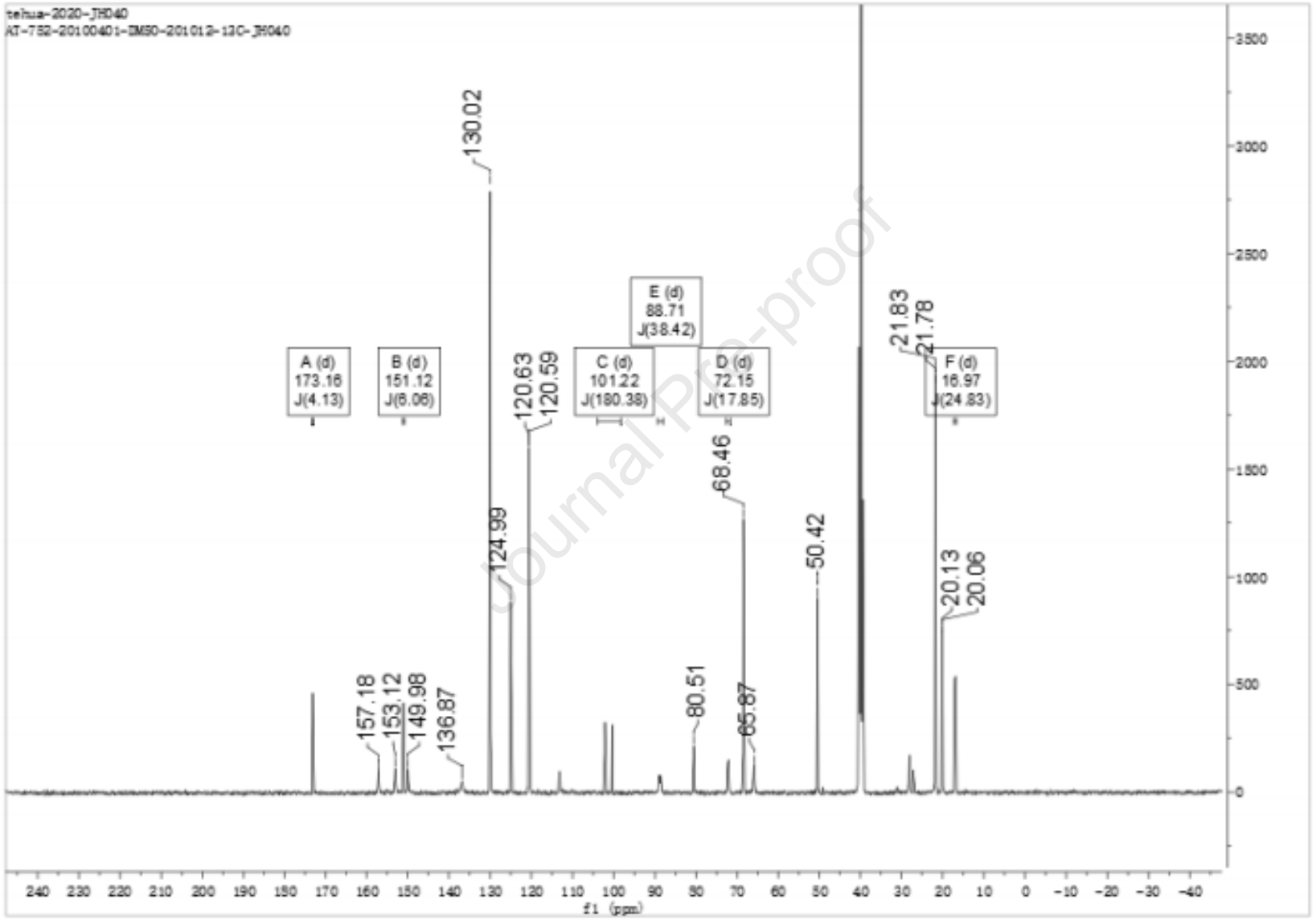

**Figure 8: AT-752 Structure Elucidation–$^{13}$C-NMR (Zoom In)**

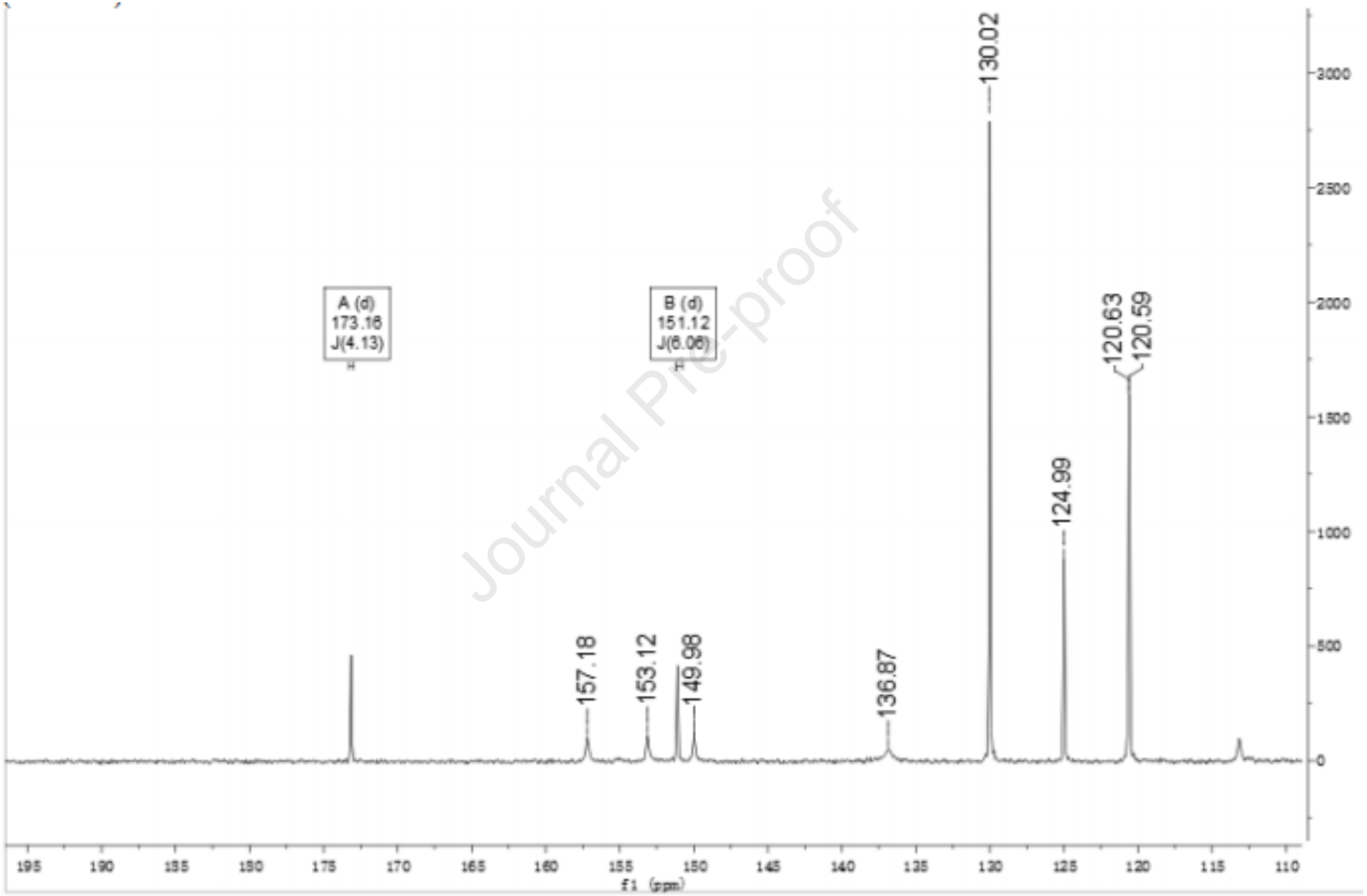

**Figure 9: AT-752 Structure Elucidation–$^{13}$C-NMR (Zoom In, continued)**

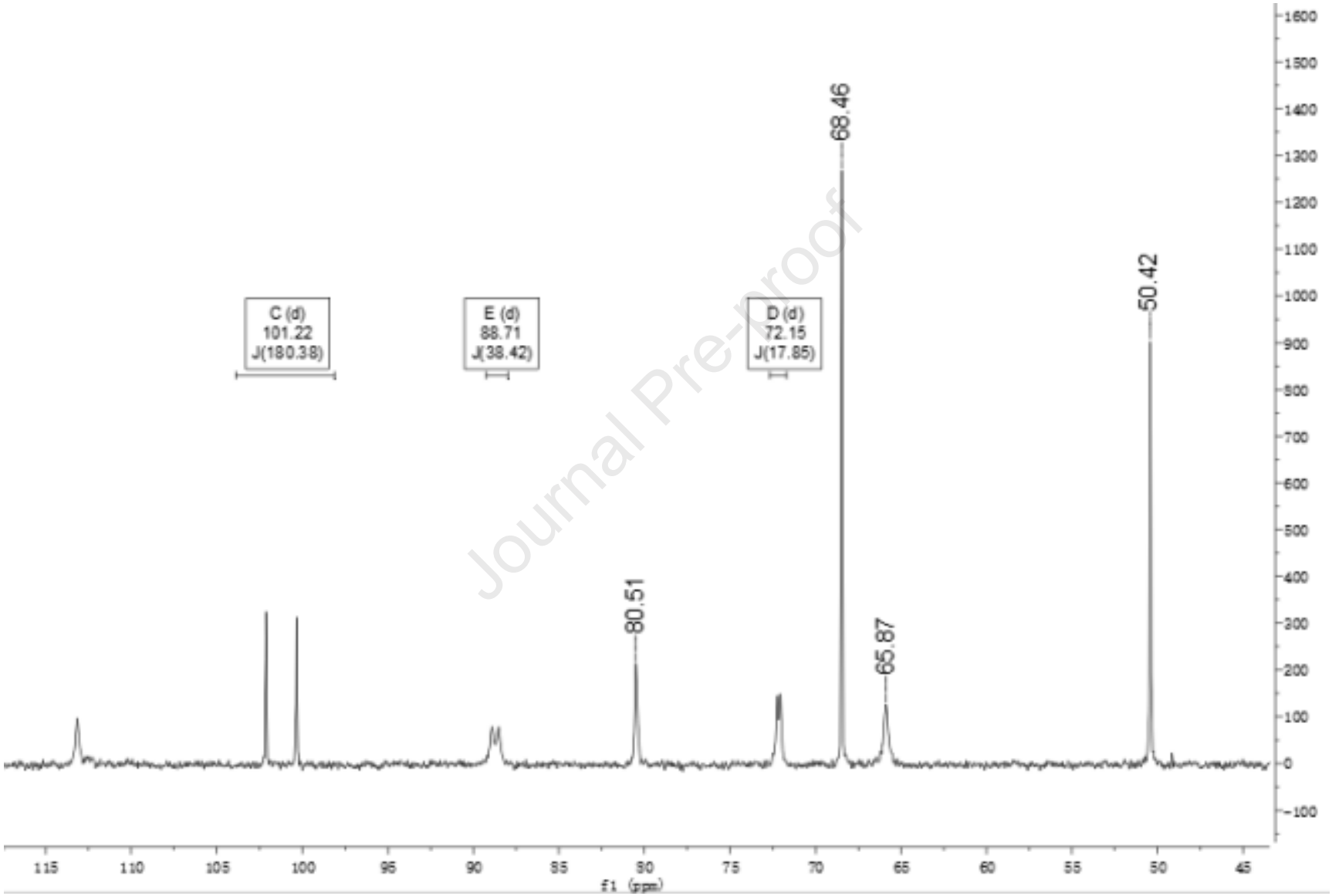

**Figure 10: AT-752 Structure Elucidation–$^{13}$C-NMR (Zoom In, continued)**

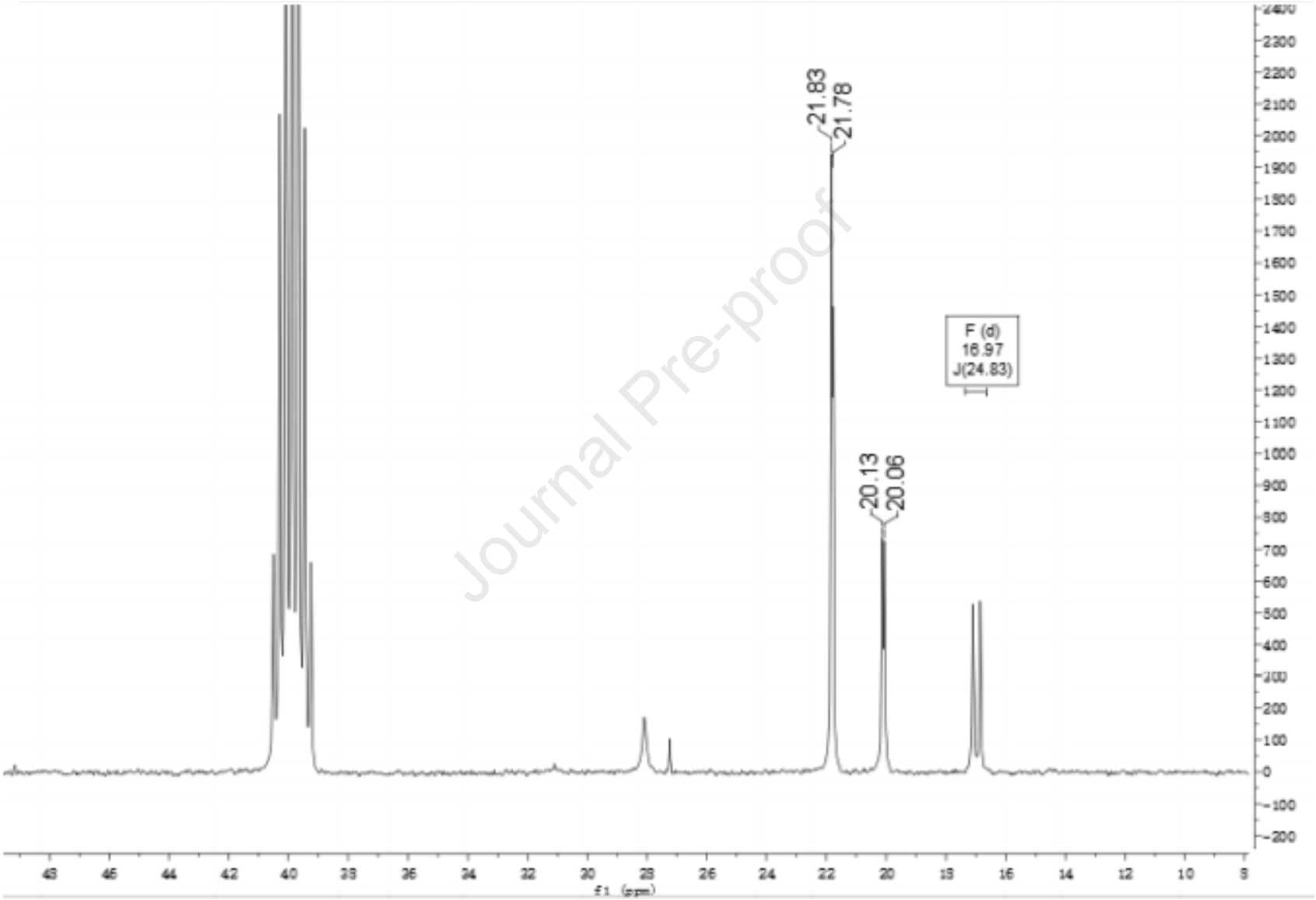

**Table 2: $^{13}$C-NMR Results (in DMSO-*d*6)**

| Number | Chemical shift δ (ppm) | Carbon Type | Peak Assignment |
|---|---|---|---|
| 1. | 173.16 | Quaternary | C-3<br>d, $J_{C-P}$ = 4.13 Hz |
| 2. | 157.18 | Quaternary | C-25 |
| 3. | 153.12 | Quaternary | C-20 |
| 4. | 151.12 | -CH | C-17<br>d, $J_{C-F}$ = 6.19 Hz |
| 5. | 149.98 | Quaternary | C-22 |
| 6. | 136.87 | Quaternary | C-23 |
| 7. | 130.02 | -CH | C-8 |
| 8. | 124.99 | -CH | C-9 |
| 9. | 120.61 | -CH | C-7<br>d, $J_{C-P}$ = 4.73 Hz |
| 10. | 113.15 | Quaternary | C-24 |
| 11. | 101.22 | Quaternary | C-13<br>d, $J_{C-F}$ = 180.38 Hz |
| 12. | 88.71 | -CH | C-14<br>d, $J_{C-F}$ = 40.83 Hz |
| 13. | 80.48 | -CH | C-11<br>d, $J_{C-F}$ = 5.99 Hz |
| 14. | 72.15 | -CH | C-12<br>d, $J_{C-F}$ = 17.85 Hz |
| 15. | 68.46 | -CH | C-4 |
| 16. | 65.87 | $-CH_2$ | C-10 |
| 17. | 50.42 | -CH | C-2 |
| 18. | 21.83 | $-CH_3$ | C-1 |
| 19. | 21.78 | $-CH_3$ | C-1 |
| 20. | 20.13 | $-CH_3$ | C-5 |
| 21. | 20.06 | $-CH_3$ | C-19 |
| 22. | 16.97 | $-CH_3$ | C-16<br>d, $J_{C-F}$ = 24.83 Hz |

## 2. MASS SPECTROMETRY

Mass Spectrometry (MS) analysis is presented in Figure 11. The peak with highest intensity at m/z 582.08 corresponds to molecular ion peak $[M+H]^+$ of AT--752 (free base form).

**Figure 11: AT-752 Structure Elucidation - MS Spectrum of AT-752 Lot 20100401**

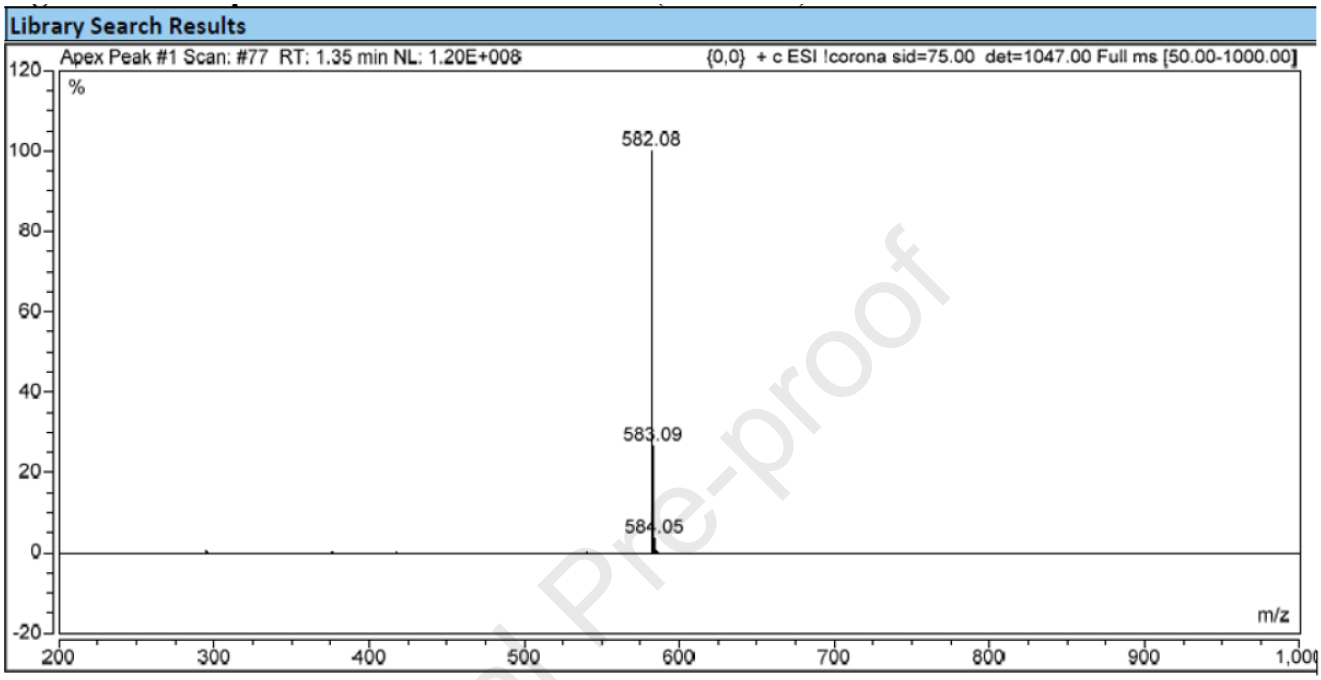


## 3. HPLC ANALYSIS

Column: XSelect CSH C18 4.6×150mm,3.5μm

Mobile Phase A: Mobile phase A: 0.01mol/L diammonium phosphate (PH6.5) (Weigh1.32g of diammonium phosphate, add 950ml of water to dissolve, adjust the pH to 6.5 with phosphoric acid, dilute to 1000ml, filter with 0.45μm membrane, then degas.)

Mobile Phase B: Acetonitrile and Methanol (2:3)

Gradient Elution

| Time (min) | A | B |
|---|---|---|
| 0 | 60 | 40 |
| 20 | 40 | 60 |
| 25 | 20 | 80 |
| 35 | 20 | 80 |

| | | |
|---|---|---|
| 35.1 | 60 | 40 |
| 42 | 60 | 40 |

Column Temperature: 30 ˚C

Detector: UV, 220 nm

Injection: 10µL

Flow Rate: 0.8 mL/min

Diluent: Methanol

Solution Preparation

Standard Solution:

Accurately weigh 25mg of AT-752 standard into a 25ml volumetric flask, dissolve with and dilute to the volume with diluent. Pipette 2ml of the above solution to a 10ml volumetric flask, and dilute with diluent to the volume. (With AT-752 about 0.2mg/mL)

Sample solution

Take the sample (concentration is about 1g/5ml acetone solution) and dilute it with methanol to the point when AT-281 is 0.2mg/ml.

Injection Sequence

Diluent

Standard solution (x3) – Inject 3 needles, RSD ⩽ 1.0%

Sample solution (x2) – Inject 2 needles.

Analysis

AT-281 %= $\frac{A_{Sas} \times C_{ss}}{A_{ss} \times C_{sas}} \times 100$

Where:

| | |
|---|---|
| CSS | Concentration of AT-281 in standard solution, mg/ml |
| CSaS | Concentration of sample solution, mg/ml |
| ASS | Average peak area in the chromatogram of the standard solution. |
| ASaS | Peak area in chromatogram of the sample solution. |

Css is calculated as formula below:

Css = $\frac{\boldsymbol{W_{ss}}\times\boldsymbol{P}\times(\mathbf{100\%}-\boldsymbol{sulfate}\%)}{\mathbf{125}}$

Where:

| | |
|---|---|
| WSS | = Weight of AT-752 in standard, mg |
| P | = Content of AT-752 Standard |
| Sulfate% | = Sulfuric acid content in the standard |
| 125 | = Diluted volume of the standard, mL |

73
74

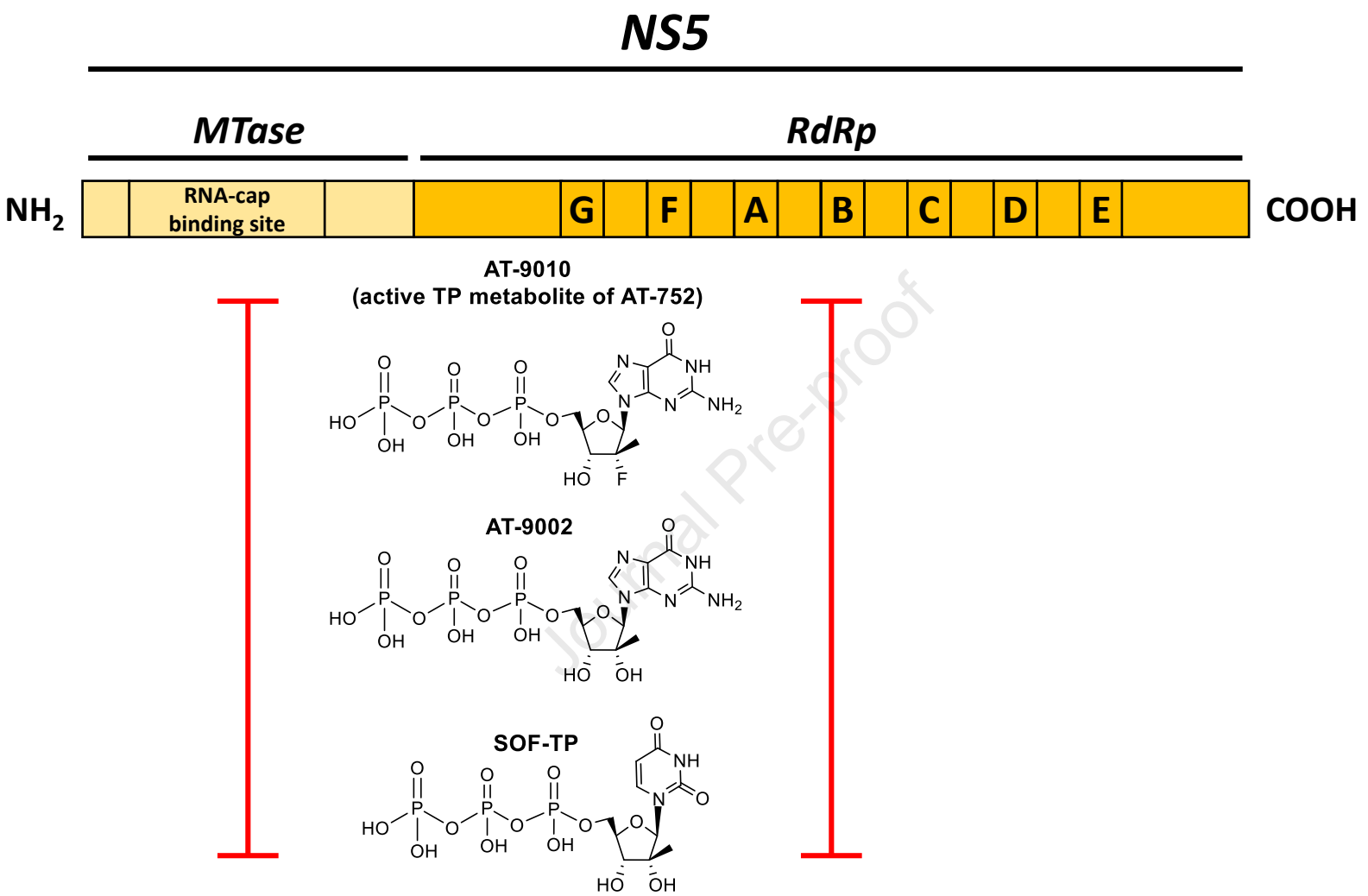


Figure 1

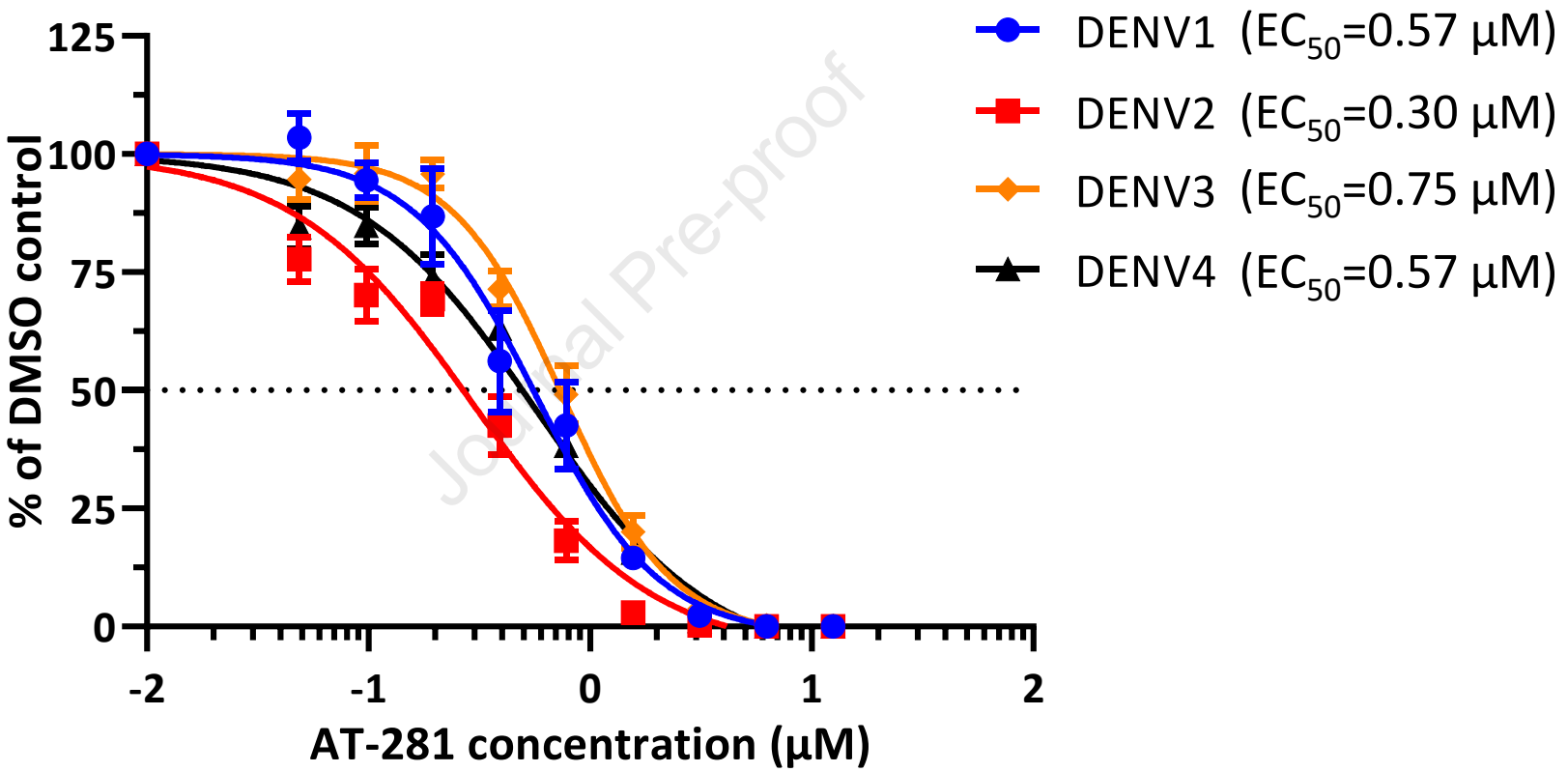


Figure 2

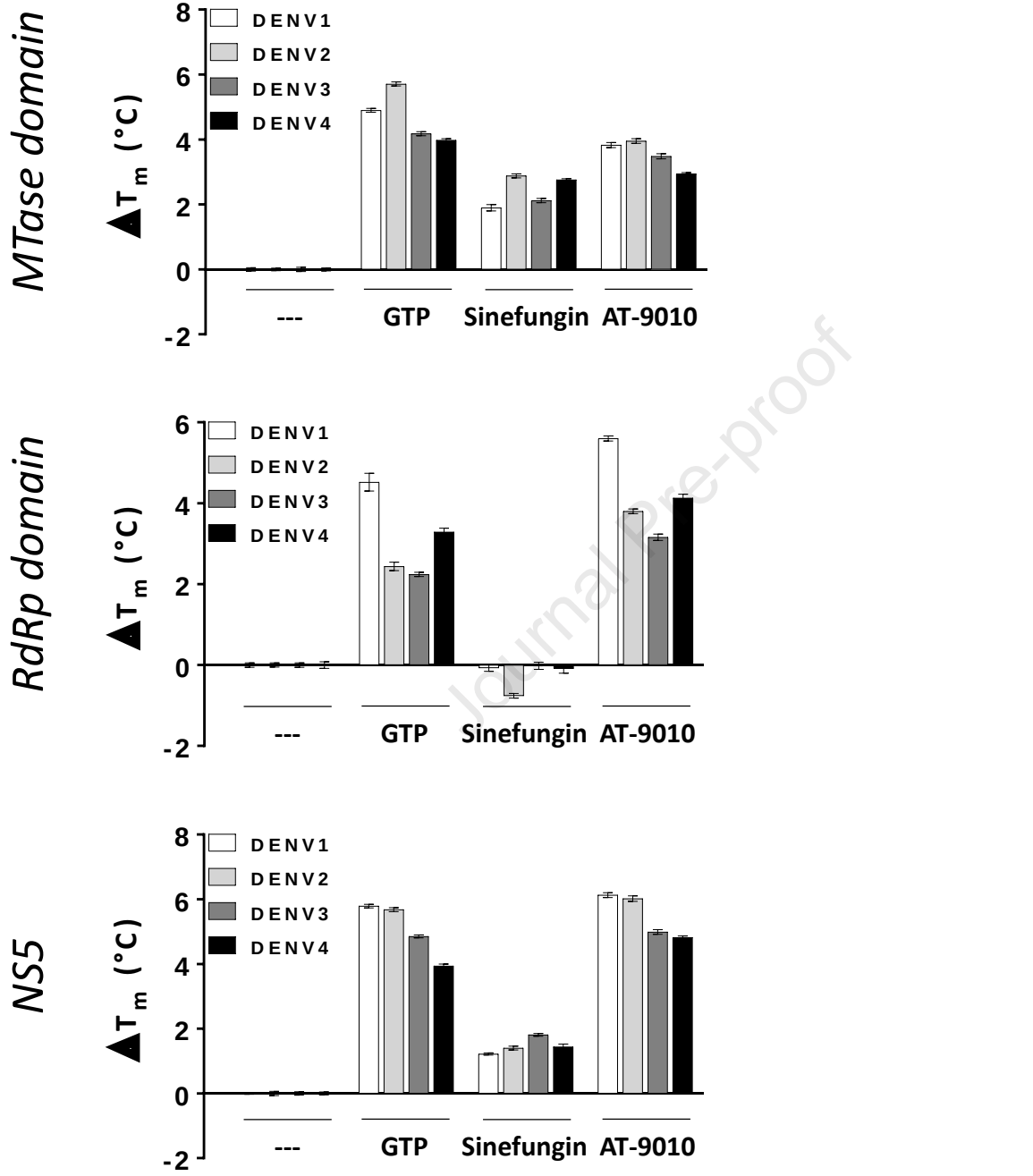




Figure 3

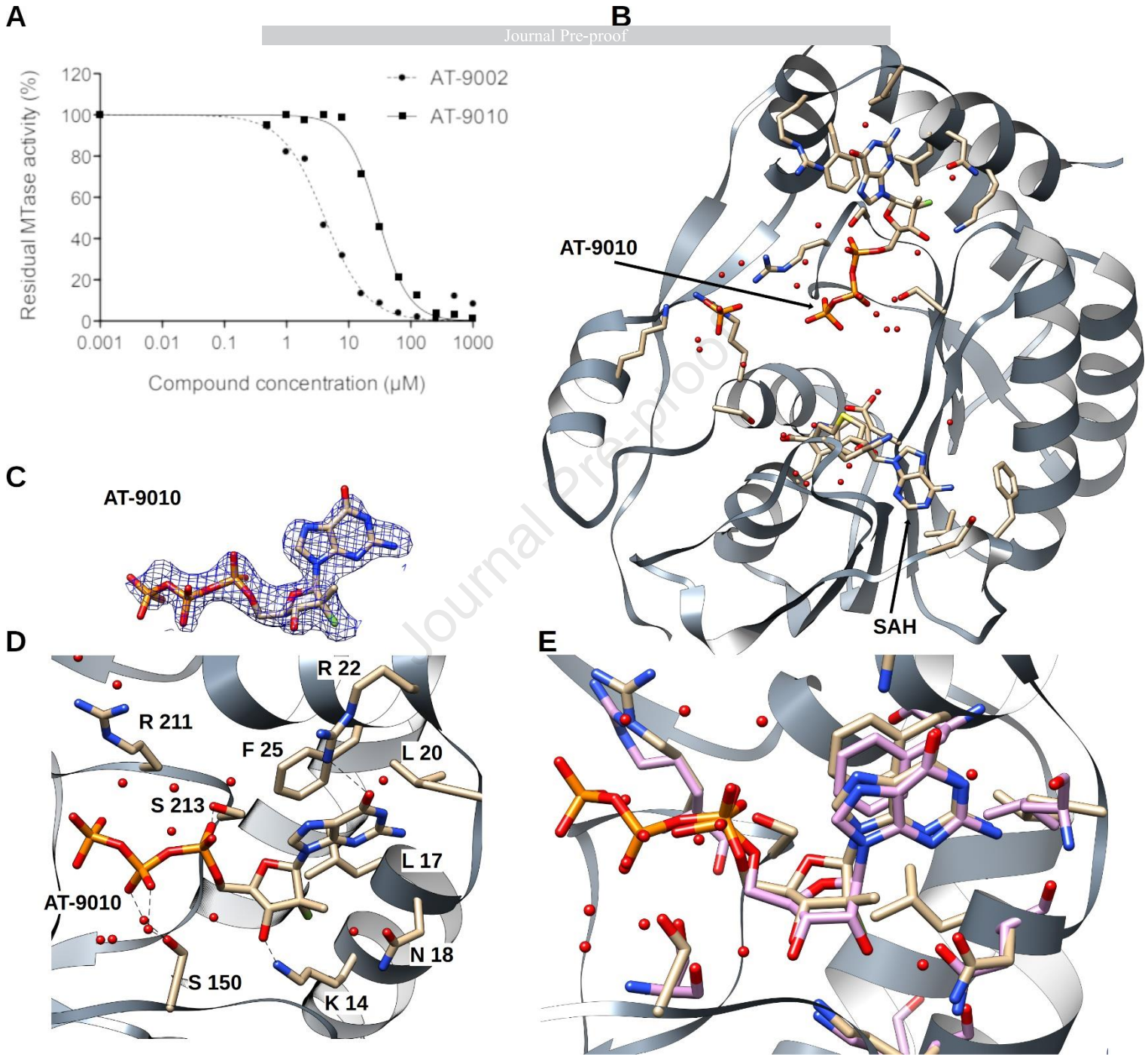


Figure 4

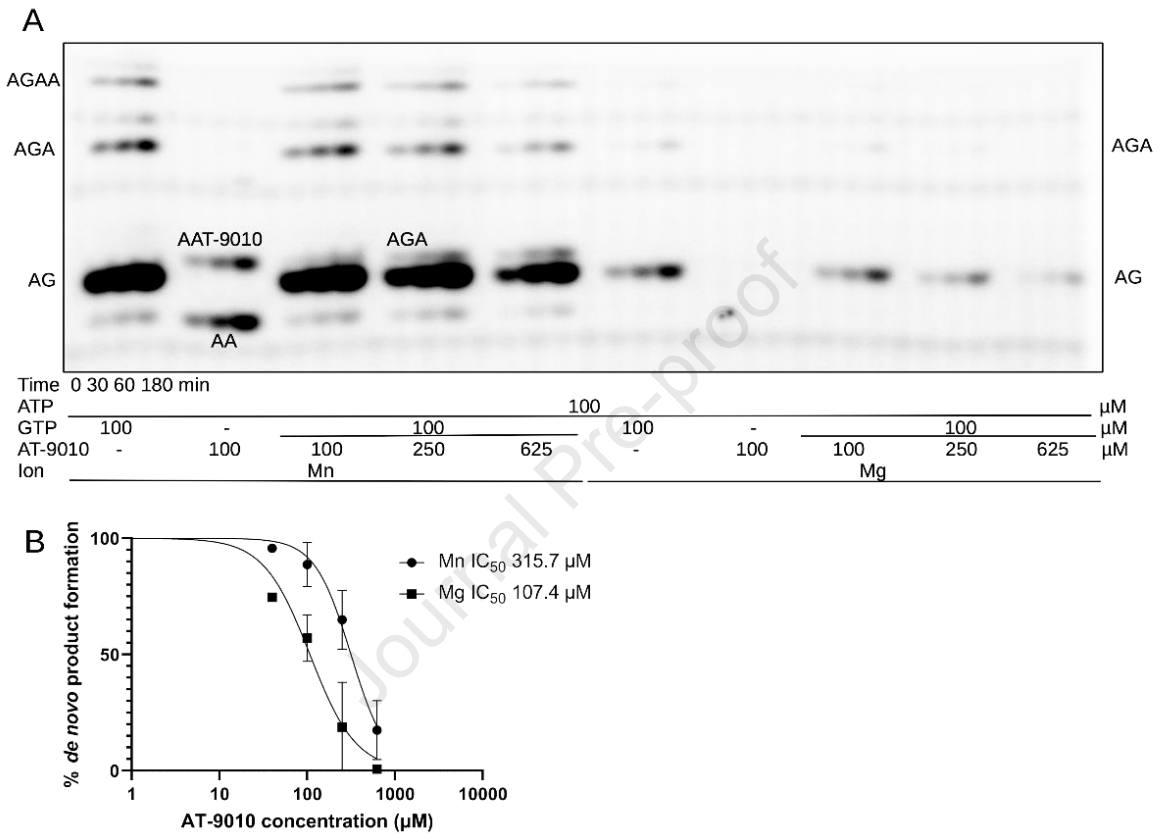
A
AGAA
AGA
AG
AAT-9010
AGA
AA
AGA
AG
Time 0 30 60 180 min
ATP 100 µM
GTP 100 - 100 100 - 100 µM
AT-9010 - 100 100 250 625 - 100 100 250 625 µM
Ion Mn Mg
B
% de novo product formation
100
50
0
1
10
100
1000
10000
AT-9010 concentration (µM)
Mn IC50 315.7 µM
Mg IC50 107.4 µM

Figure 5

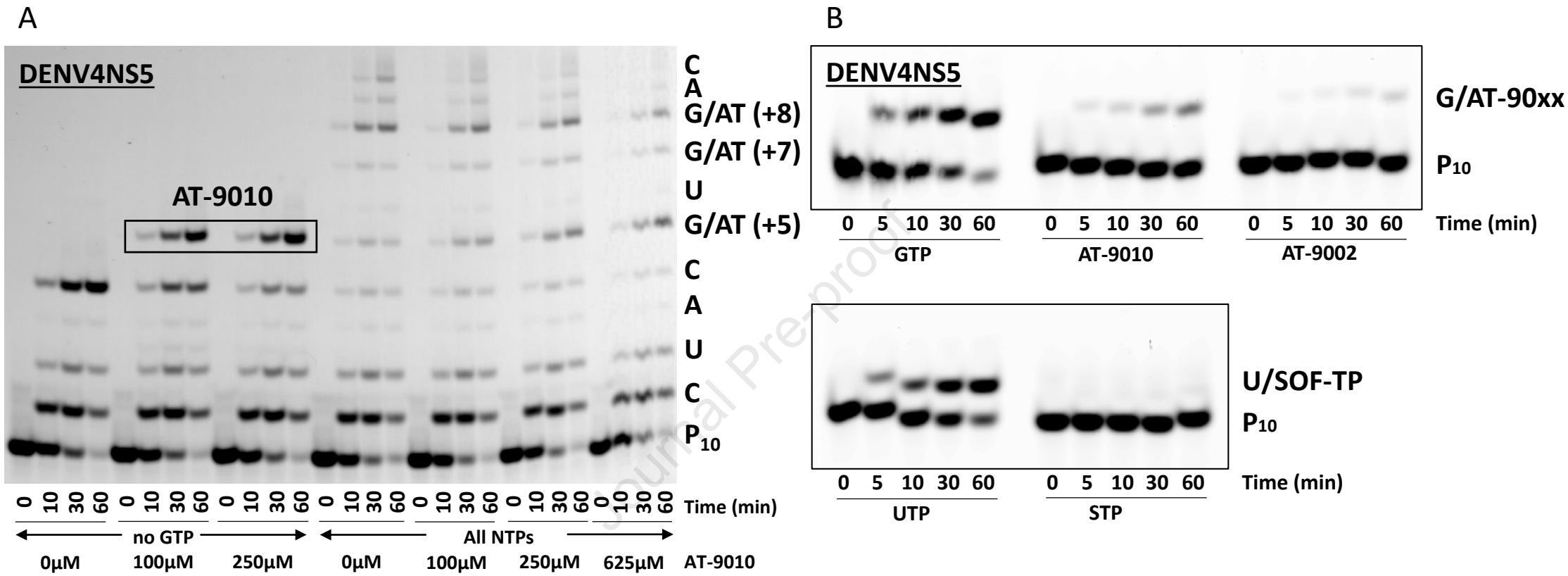


Figure 6

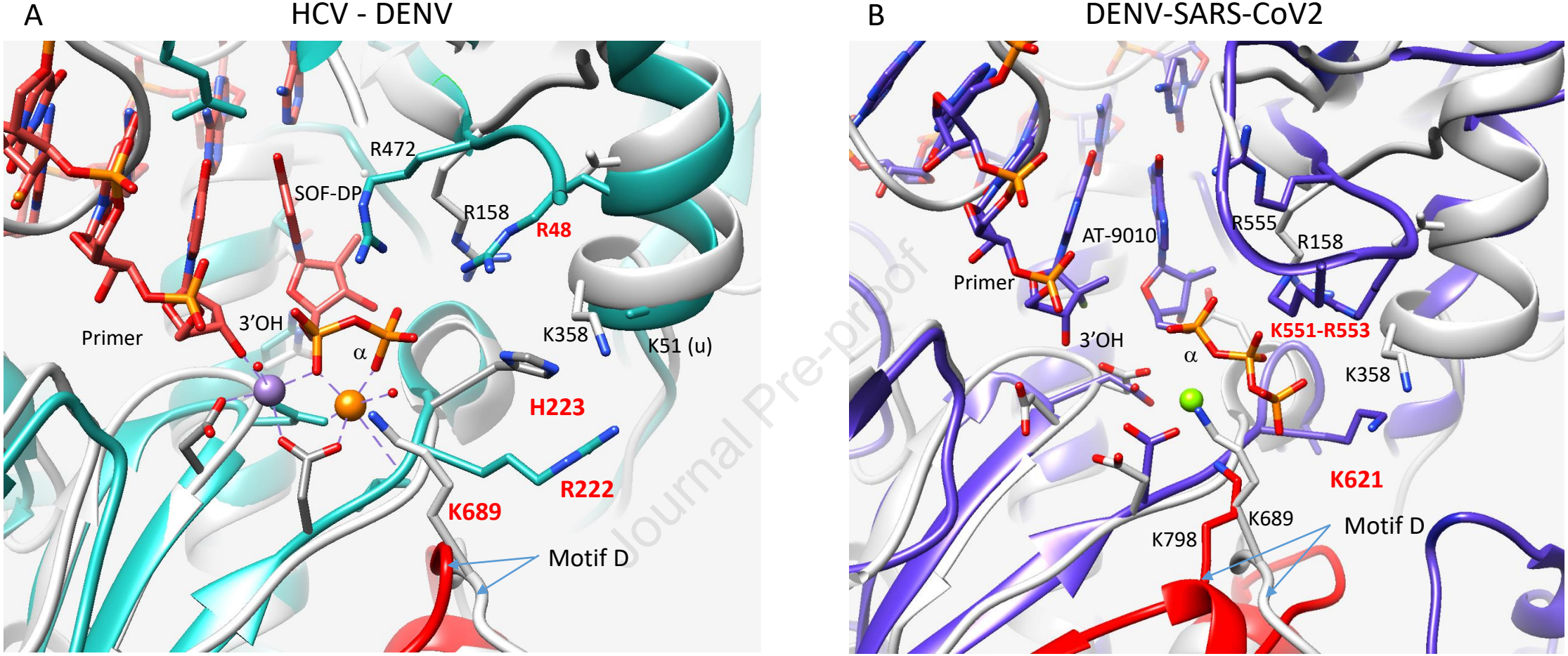


Figure 7

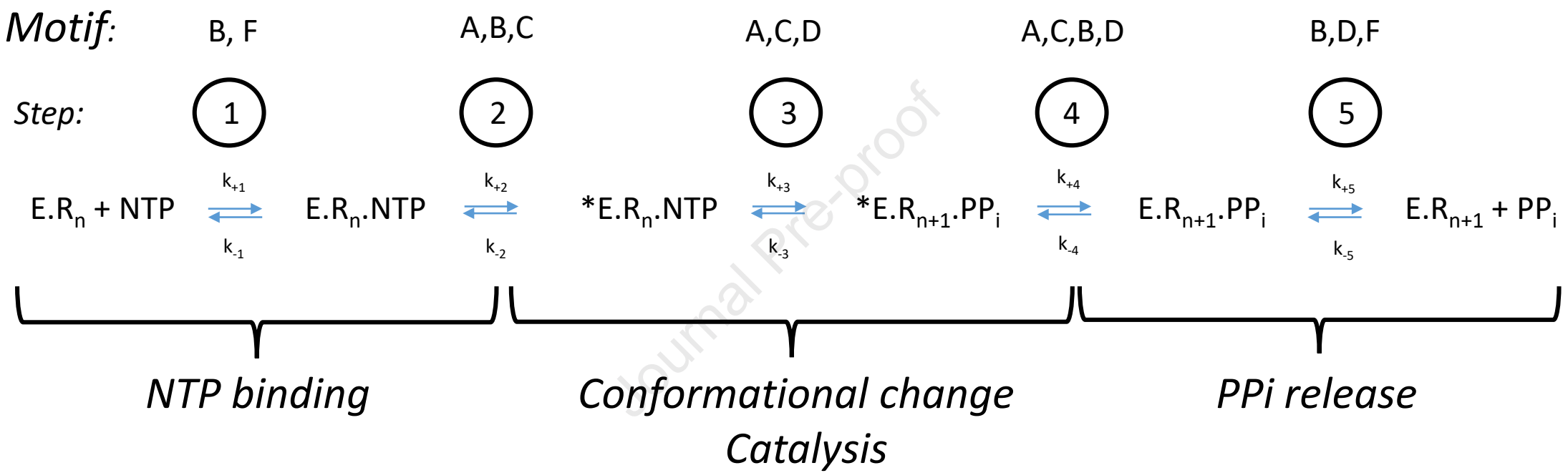


Scheme 1

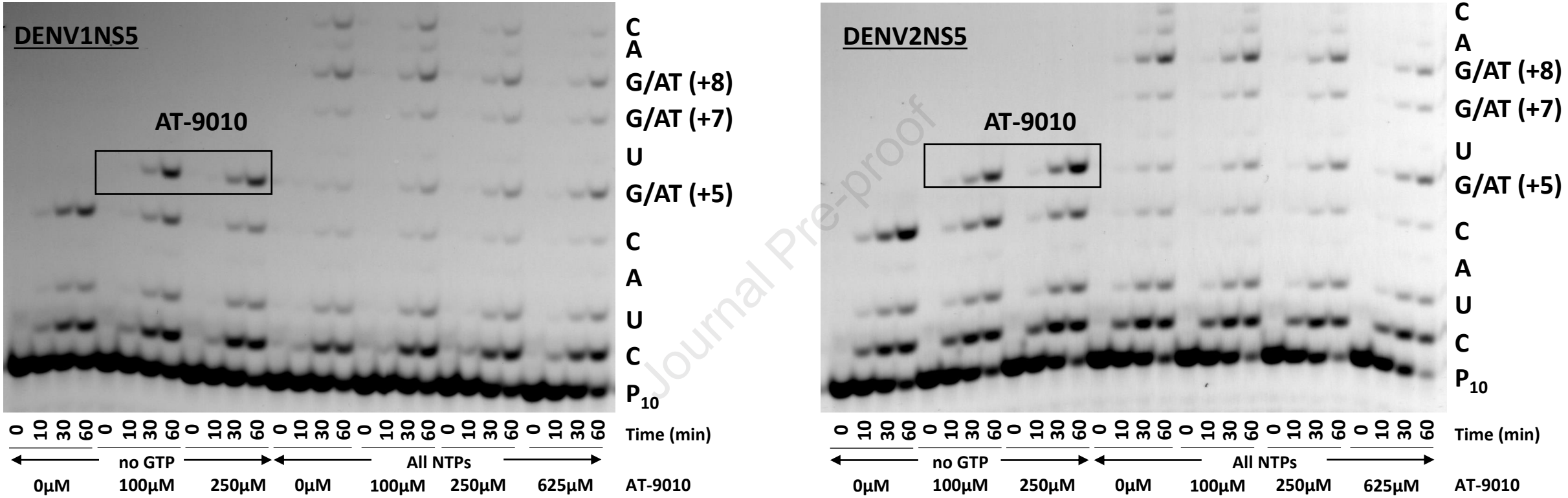




Supplementary Fig. 1A

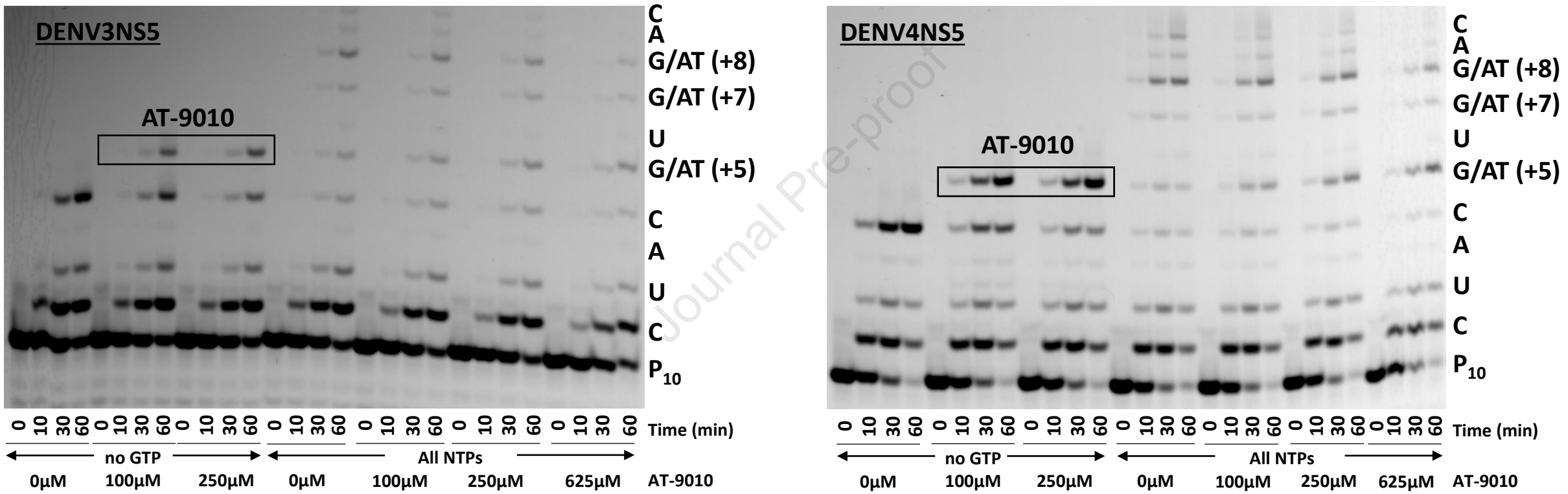




Supplementary Fig. 1B

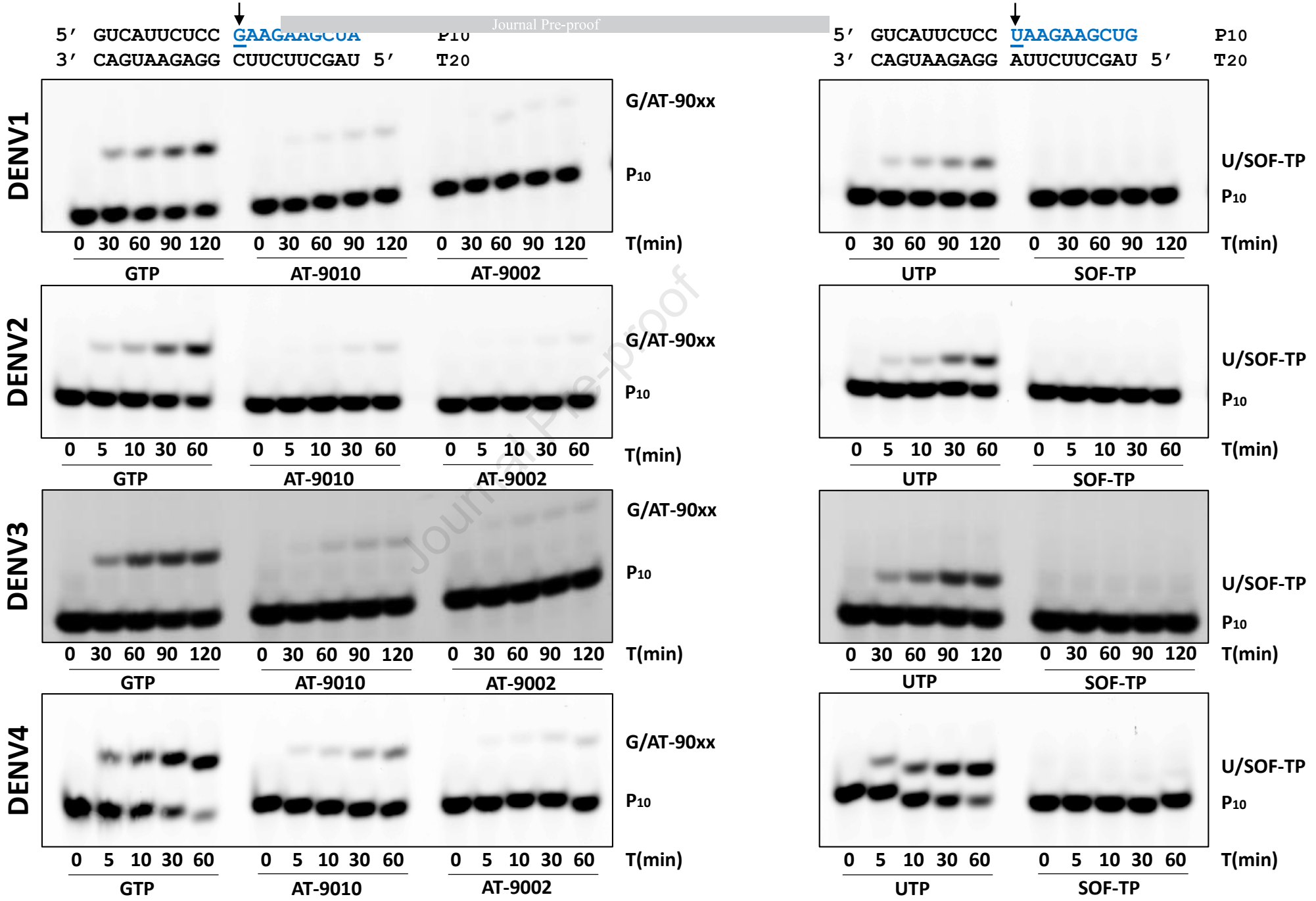


Supplementary Fig. 2

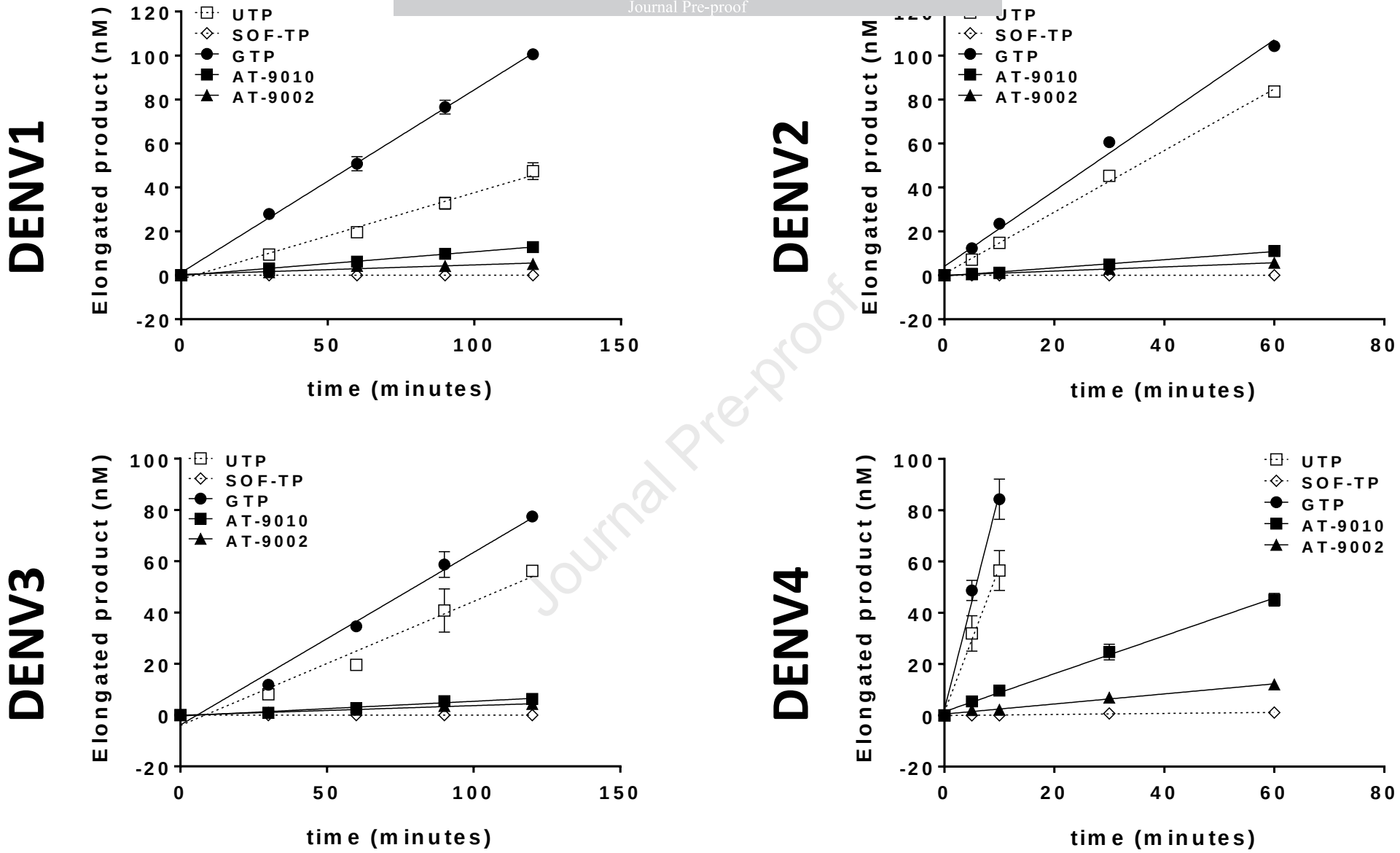




Supplementary Fig. 3

Highlights

- AT-752 prodrug active against Dengue virus serotype 1-4 , with $EC_{50} \approx 0.50$ μM
- Active drug AT-9010 has dual activity as chain-terminator and 2'-O-MTase inhibitor
- Xtal structure of DENV NS5 MTase at 1.97 Å shows AT-9010 in conserved binding site
- Motif D lys and purine stacking explains better potency AT-752 than Sofosbuvir